

Integrated Sensing and Communications in Clutter Environment

Hongliang Luo, Yucong Wang, Dongqi Luo, Jianwei Zhao, Huihui Wu, Shaodan Ma and Feifei Gao

Abstract—In this paper, we propose a practical integrated sensing and communications (ISAC) framework to sense dynamic targets from clutter environment while ensuring users communications quality. To implement communications function and sensing function simultaneously, we design multiple communications beams that can communicate with the users as well as one sensing beam that can rotate and scan the entire space. To minimize the interference of sensing beam on existing communications systems, we divide the service area into *sensing beam for sensing (S4S) sector* and *communications beam for sensing (C4S) sector*, and provide beamforming design and power allocation optimization strategies for each type sector. Unlike most existing ISAC studies that ignore the interference of static environmental clutter on target sensing, we construct a mixed sensing channel model that includes both static environment and dynamic targets. When base station receives the echo signals, it first filters out the interference from static environmental clutter and extracts the effective dynamic target echoes. Then a complete and practical dynamic target sensing scheme is designed to detect the presence of dynamic targets and to estimate their angles, distances, and velocities. In particular, dynamic target detection and angle estimation are realized through angle-Doppler spectrum estimation (ADSE) and joint detection over multiple subcarriers (MSJD), while distance and velocity estimation are realized through the extended subspace algorithm. Simulation results demonstrate the effectiveness of the proposed scheme and its superiority over the existing methods that ignore environmental clutter.

Index Terms—Integrated sensing and communications, dynamic target sensing, static environment sensing, clutter suppression, power allocation.

I. INTRODUCTION

Integrated sensing and communications (ISAC) has recently attracted significant research interest in the field of wireless communications [1]–[3]. The idea is to utilize communication signals to sense various information in real physical world, such as architectural composition, human activity, etc, while ensuring users communications quality. Since ISAC allows sensing systems and communication systems to share the same hardware and spectrum resources, and can serve various intelligent applications, such as vehicle-to-everything, digital twins, etc., it has been deemed as one of the key technologies for sixth generation (6G) communications [4], [5].

Hongliang Luo, Yucong Wang, Dongqi Luo, Huihui Wu and Feifei Gao are with Department of Automation, Tsinghua University, Beijing 100084, China (email: luohl23@mails.tsinghua.edu.cn; wanguyuc21@mails.tsinghua.edu.cn; dongqiluo@gmail.com; hhwu1994@mail.tsinghua.edu.cn; feifeigao@ieee.org).

Jianwei Zhao is with the High-Tech Institute of Xi'an, Xi'an 710025, China (e-mail: zhaojianeip@163.com).

Shaodan Ma is with the State Key Laboratory of Internet of Things for Smart City and the Department of Electrical and Computer Engineering, University of Macau, Macao S.A.R. 999078, China (e-mail: shaodanma@um.edu.mo).

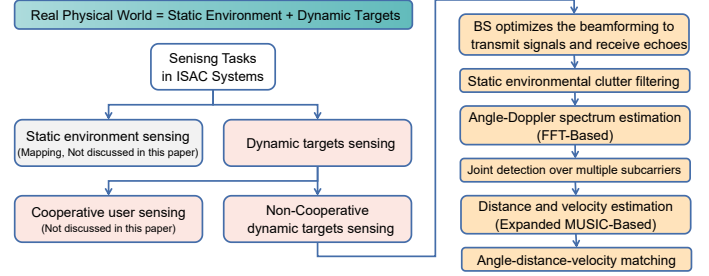


Fig. 1. ISAC sensing task classification and flowchart of the proposed sensing echo signals processing process.

The ultimate functionality of sensing is to construct the mapping relationship from *real physical world* to *digital twin world*, where the former includes static environment (such as roads and buildings) and dynamic targets (such as pedestrians and vehicles). Therefore, sensing tasks in ISAC systems include *static environment sensing (SES)* and *dynamic targets sensing (DTS)* as shown in left half of Fig. 1. The changes of static environment are usually slow, and thus one can apply various environmental reconstruction techniques to sense static environment [6]–[8]. However, since the changes of dynamic targets are rapid, it is necessary to detect the presence of dynamic targets and update their parameter estimates in real-time. Generally, one can divide DTS problem into two categories: 1) sensing cooperative communications users, e.g., mobile phones; and 2) sensing non-cooperative dynamic targets that are not communicating with base station (BS), e.g., moving objects or mobile users not in communication status.

In addition, with the increasing demand for sensing, researchers are committed to making ISAC systems possess ultra-high sensing accuracy. Encouragingly, sensing in mmWave or Terahertz band with massive multiple input and multiple output (MIMO) array can achieve higher accuracy thanks to its high directivity and high temporal resolution [9], [10]. Therefore, the massive MIMO array based ISAC systems have been widely studied. For the aspect of sensing cooperative users, the users' positions can be estimated by processing the communications signals and extracting the channel parameters, such as time of arrival (TOA), angle of departure (AOD), etc [11]–[14]. On the other side, sensing non-cooperative target has also been studied under ISAC framework. For example, Z. Gao *et al.* proposed an ISAC system relying on MIMO array, which applied compressed sampling to facilitate target sensing and other ISAC processing [15]. Z. Wang *et al.* proposed a simultaneously transmitting and reflecting surface enabled ISAC framework, in which the

two-dimensional maximum likelihood estimation was utilized to estimate target angle [16]. Y. Li *et al.* proposed a two-stage algorithm to estimate the positions and velocities of multiple targets with orthogonal frequency division multiplexing (OFDM) signals [17]. P. Kumari *et al.* proposed an ISAC system working for the internet of vehicles, which realized vehicle to vehicle communication and full duplex radar sensing [18]. X. Chen *et al.* proposed a multiple signal classification based ISAC system that can attain high estimation accuracy for dynamic target sensing [19]. However, all these works ignore the interference caused by static environmental clutter on dynamic target sensing, which does not match the real scenarios where the targets are always submerged by the interference of static environment and are difficult to separate from it, thus limiting the sensing performance in the real scenarios and practical ISAC systems.

Meanwhile, for ISAC systems based on MIMO arrays, one should design the beamforming with multiple beams to implement communications function and sensing function simultaneously [20]–[23]. For example, C. B. Barneto *et al.* formulated one beamforming design problem in multi-user ISAC system, aiming to maximize the power at the sensing direction while remain certain power at the communications directions [24]. H. Luo *et al.* proposed an ISAC system that combined BS and reconfigurable intelligence surface (RIS), and optimized the beamforming matrix jointly to maximize the achievable sum-rate of communication users while meeting the sensing beam constraints [25]. X. Wang *et al.* investigated the partially-connected beamforming design for multi-user ISAC systems, aiming to minimize the Cramer-Rao bound of DOA estimation while ensuring communications performance [26]. However, all these works require complex optimization processes and are difficult to implement in practical systems.

Based on the above analysis, the existing researches on ISAC systems require complex optimization solutions in beamforming design and ignore the serious interference of environmental clutter in echo signal processing, making it difficult to deploy and apply in actual BS systems. In this paper, we propose a practical ISAC framework to sense the dynamic targets from the clutter environment while ensuring users communications quality. The contributions of this paper are summarized as follows.

- We propose a practical ISAC framework to implement communications and sensing simultaneously, in which we design multiple communications beams that can communicate with the users while assign one sensing beam that can rotate and scan the entire space. The entire process is summarized in the right half of Fig. 1.
- BS should optimize the transmitting beamforming during each time slot to transmit signals. Specifically, to minimize the interference of sensing beam on existing communications systems, we divide the service area of BS into *sensing beam for sensing (S4S) sectors* and *communications beam for sensing (C4S) sectors*. To avoid complex optimizations that are difficult to implement in practical systems, we transform the precoding optimization problem into a power allocation problem for communications and sensing beams, and provide effective

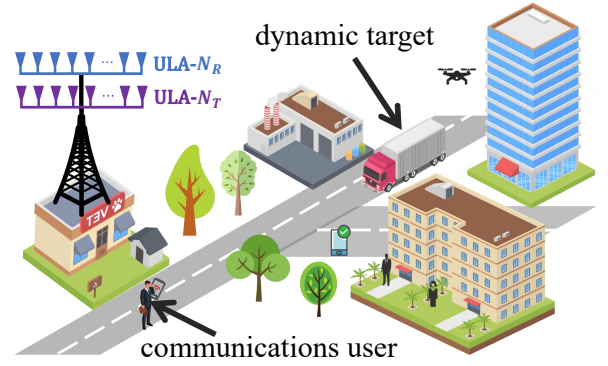


Fig. 2. System model.

power allocation strategies for each type sector.

- We construct clutter environment model for practical ISAC systems, and then the echoes received by BS includes both the echoes caused by static environment and the echoes caused by dynamic targets. To address the negative interference of static environmental clutter on dynamic target sensing, we first filter out the interference from static environmental clutter and extract the effective dynamic target echoes. Then angle-Doppler spectrum estimation (ADSE) and joint detection over multiple sub-carriers (MSJD) are proposed to detect dynamic targets and to estimate their angles. The extended subspace algorithm is utilized to estimate distances and velocities of dynamic targets. Besides, in order to obtain multiple parameters for each target, we design an angle-distance-velocity matching method to realize parameters matching.
- Various simulations are provided to demonstrate the effectiveness of the proposed schemes and its superiority over existing methods that ignore environmental clutter.

The remainder of this paper is organized as follows. In Section II, we propose a practical ISAC framework that effectively integrates the sensing functions into the existing communications systems. In Section III, we provide a low complexity and practical beamforming design and power allocation strategy. Then we design a complete and practical scheme to sense the dynamic targets from the clutter environment in Section IV. Simulation results and conclusions are given in Section V and Section VI, respectively.

Notation: Lower-case and upper-case boldface letters \mathbf{a} and \mathbf{A} denote a vector and a matrix; \mathbf{a}^T and \mathbf{a}^H denote the transpose and the conjugate transpose of vector \mathbf{a} , respectively; $\mathbf{a}[n]$ denotes the n -th element of the vector \mathbf{a} ; $\mathbf{A}[i, j]$ denotes the (i, j) -th element of the matrix \mathbf{A} ; $\mathbf{A}[i_1 : i_2, :]$ is the submatrix composed of all columns elements in rows i_1 to i_2 of matrix \mathbf{A} ; $\mathbf{A}[:, j_1 : j_2]$ is the submatrix composed of all rows elements in columns j_1 to j_2 of matrix \mathbf{A} ; $|\cdot|$ denotes the absolute operator; $\text{eig}(\cdot)$ represents the matrix eigenvalue decomposition function. \mathbb{R} and \mathbb{C} represent the real field and complex field, respectively. $\mathbb{E}\{\cdot\}$ is the mathematical expectation operator.

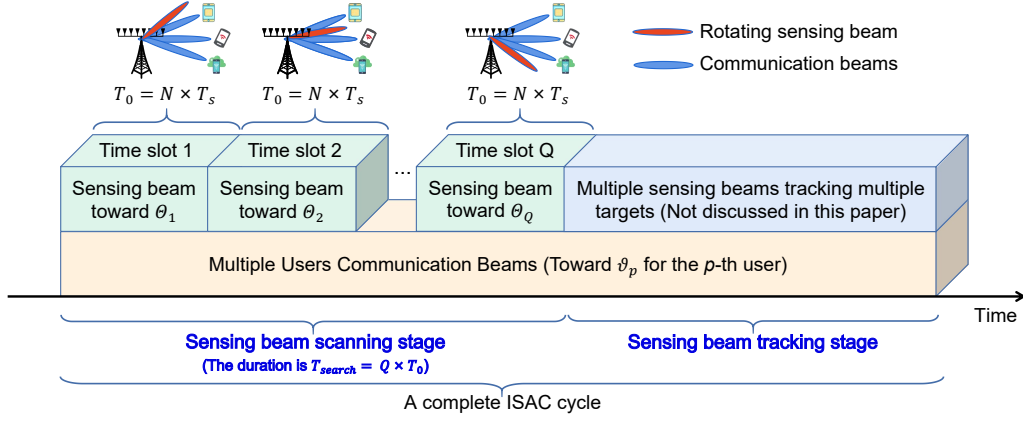


Fig. 3. The proposed ISAC framework.

II. SYSTEM MODEL AND PROPOSED ISAC FRAMEWORK

In this section, we will propose a practical ISAC framework that effectively integrates the sensing functions into the existing communications systems.

A. BS Model

A massive MIMO based ISAC system operating in mmWave or Terahertz frequency bands with OFDM modulation is depicted in Fig. 2, which employs a dual function BS for wireless communication and radar sensing at the same time. The BS is configured with two parallel and closely placed uniform linear arrays (ULAs) of N_T and N_R antenna elements as transmitting array and receiving array, respectively, in which the antenna spacing is $d \leq \frac{\lambda}{2}$ and λ is the wavelength. Assuming that the ULAs are parallel to the y-axis, and the antenna indices in the transmitting- and receiving- ULAs are $0, \dots, N_T - 1$ and $0, \dots, N_R - 1$. Suppose that the communications system uses narrowband OFDM signals with M subcarriers in total, and the lowest frequency and the subcarrier interval are f_0 and Δf , respectively. Then the transmission bandwidth is $W = (M - 1)\Delta f$, and the frequency of the m -th subcarrier is $f_m = f_0 + m\Delta f$, where $m = 0, 1, \dots, M - 1$.

Assume that the service area of BS is $\{(r, \theta) | r_{min} \leq r \leq r_{max}, \theta_{min} \leq \theta \leq \theta_{max}\}$, and there are P single-antenna communications users, K dynamic targets, as well as widely distributed static environment within this area. We assume that the position and radial velocity of the k -th dynamic target are (r_k, θ_k) and v_k . Besides, we assume that the position of the p -th user is (R_p, ϑ_p) , and suppose that the positions of users are known and are stationary to BS, as the cooperative users' positions can be easily obtained through user reporting, or other techniques [9], [10], [27].

B. Proposed ISAC Framework

The task of an ISAC system is to sense all K dynamic targets while serving the communications of all P users, in which the sensing of dynamic targets includes detection, estimation, and tracking. As described in Fig. 3, the proposed ISAC framework consists of two stages: *sensing beam scanning (SBS) stage* and *sensing beam tracking (SBT) stage*. For

the aspect of communications, BS continuously generates P communications beams towards P users to maintain communications service during both SBS stage and SBT stage.

For the aspect of sensing, BS generates one sensing beam that can rotate and scan the service area during SBS stage, that is, the sensing beam can explore all angle spaces at certain scanning intervals within a certain period of time, and BS can detect the targets and estimate their parameters during SBS stage. Next, BS should generate one or K sensing beams to track all K dynamic targets during SBT stage. In this work, we mainly focus on SBS stage, while SBT stage is a well separate issue and will be discussed in subsequent works.

Suppose that BS adopts N consecutive OFDM symbols to realize dynamic target sensing in one single direction, and OFDM symbol interval time is $T_s = \frac{1}{\Delta f}$. As shown in Fig. 3, we divide the SBS stage into Q transient time slots, and each time slot lasts for a time duration of $T_0 = N \cdot T_s$. In the q -th time slot, BS needs to generate P communications beams pointing to P users and generate one sensing beam pointing to the *sensing scanning angle* Θ_q from transmitting array. Here we assume that the transmission power of BS is P_t , the energy of sensing beam is $\rho_q^s P_t$ with $\rho_q^s \in [0, 1]$, the energy of communications beam for the p -th user is $\rho_{q,p}^c P_t$ with $\rho_{q,p}^c \in [0, 1]$, where $p = 1, 2, \dots, P$, and there is $\rho_q^s + \sum_{p=1}^P \rho_{q,p}^c = 1$. We collectively refer to $\rho_q^s, \rho_{q,1}^c, \rho_{q,2}^c, \dots, \rho_{q,P}^c$ as the *power allocation factor*. Then the transmission signals on the m -th subcarrier of the n -th OFDM symbol in the q -th time slot should be represented as

$$\begin{aligned} \mathbf{x}_{q,n,m} &= \sum_{p=1}^P \mathbf{w}_{c,p,q} s_{n,m}^{c,p,q} + \mathbf{w}_{s,q} s_{n,m}^{s,q} \\ &= \sum_{p=1}^P \sqrt{\frac{\rho_{q,p}^c P_t}{N_T}} \mathbf{a}_{TX}(\vartheta_p) s_{n,m}^{c,p,q} + \sqrt{\frac{\rho_q^s P_t}{N_T}} \mathbf{a}_{TX}(\Theta_q) s_{n,m}^{s,q}, \end{aligned} \quad (1)$$

where $\mathbf{w}_{c,p,q} = \sqrt{\frac{\rho_{q,p}^c P_t}{N_T}} \mathbf{a}_{TX}(\vartheta_p)$ and $\mathbf{w}_{s,q} = \sqrt{\frac{\rho_q^s P_t}{N_T}} \mathbf{a}_{TX}(\Theta_q)$ are the communications beamforming vector for the p -th user and the sensing beamforming vector for the Θ_q , respectively, and $\mathbf{a}_{TX}(\theta)$ is the transmitting steering vector for angle θ with

$$\mathbf{a}_{TX}(\theta) = [1, e^{j2\pi f_0 \frac{d \sin \theta}{c}}, \dots, e^{j2\pi f_0 \frac{(N_T-1)d \sin \theta}{c}}]^T \in \mathbb{C}^{N_T \times 1}. \quad (2)$$

Moreover, $s_{n,m}^{c,p,q}$ and $s_{n,m}^{s,q}$ are the communication signals for the p -th user and the sensing detection signals transmitted by BS through the m -th subcarrier of the n -th OFDM symbol in the q -th time slot. Without loss of generality, $s_{n,m}^{c,p,q}$ and $s_{n,m}^{s,q}$ are both assumed as zero-mean, temporally-white and wide-sense stationary stochastic process, and $s_{n,m}^{c,p,q}$ is uncorrelated with $s_{n,m}^{s,q}$. Here, both $s_{n,m}^{c,p,q}$ and $s_{n,m}^{s,q}$ are normalized to have unit power, and the actual transmission power will be calculated in the corresponding beamforming vectors.

In addition, to suppress the interference of echoes from other directions, BS also demands to set one sensing receiving beam pointing to Θ_q at receiving array. Here we set the receiving beamforming vector in the q -th time slot as $\mathbf{w}_{RX,q} = \frac{1}{\sqrt{N_R}} \mathbf{a}_{RX}(\Theta_q)$, where $\mathbf{a}_{RX}(\theta)$ is the receiving steering vector for angle θ with the form

$$\mathbf{a}_{RX}(\theta) = [1, e^{j2\pi f_0 \frac{d \sin \theta}{c}}, \dots, e^{j2\pi f_0 \frac{(N_R-1)d \sin \theta}{c}}]^T \in \mathbb{C}^{N_R \times 1}. \quad (3)$$

To evenly scan the service area, we set $\Theta_q = \arcsin[\sin \theta_{min} + (q-1) \frac{\sin \theta_{max} - \sin \theta_{min}}{Q-1}]$, where $q = 1, 2, \dots, Q$. Therefore, the total duration of beam scanning in SBS stage can be expressed as $T_{SBS} = Q \times N \times T_s$.¹ Then BS will transmit signals through transmitting array and receive echoes through receiving array during each time slot. After completing the beam scanning, we need to design efficient and accurate dynamic target sensing algorithms to detect the dynamic targets and to estimate their angles, distances, and velocities in clutter environment.

C. Interference Management

During SBS stage, due to the rotation of sensing beam, the intervals between the direction of sensing beam and directions of communications beams are constantly changing. Hence, sensing beam would bring dynamic interference to communications beams. Specifically, when the sensing scanning angle Θ_q is far from user's angle, the interference of sensing beam on communications beams is relatively small. However, when Θ_q is close to user's angle, the interference of sensing beam on communications beams is significant large. Especially when the mainlobe of sensing beam overlaps with the mainlobe of communications beam, sensing beam will cause serious interference to this communications beam. Hence we should properly control the power allocated to sensing beam and communications beams to suppress dynamic interference.

Intuitively, when Θ_q is close to ϑ_p , in order to avoid serious interference caused by sensing beam on user, BS should not generate a dedicated sensing beam at this time. Interestingly, as the communications beam for the user can also illuminate the potential targets that may exist in this direction, the communications beam would also cause echoes if there are some targets in this direction, and the BS can still utilize the echoes of communications beam itself to sense the targets. Hence we divide the service area of BS into *sensing beam for sensing (S4S) sectors* and *communications beam for sensing (C4S) sectors* as shown in Fig. 4. In general, we construct

¹Generally, the overall sensing accuracy will improve with the increase of beam scanning time, and one can adjust the beam scanning time according to the required sensing accuracy.

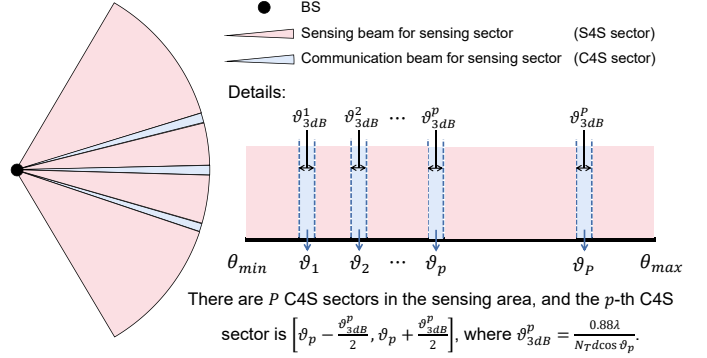


Fig. 4. Schematic diagram of S4S sector and C4S sector.

a protective C4S sector for each user, and the C4S sector corresponding to the p -th user is $[\vartheta_p - \frac{\vartheta_{3dB}^p}{2}, \vartheta_p + \frac{\vartheta_{3dB}^p}{2}]$, where $\vartheta_{3dB}^p = \frac{0.88\lambda}{N_T d \cos \vartheta_p}$ is the half power beam width². Then we should take the following strategies to suppress the interference of sensing beam on communications beams:

- 1) When Θ_q is located within the p -th C4S sector, we design that the BS does not generate the dedicated sensing beam, but utilizes the communications beam toward ϑ_p to illuminate the potential targets and realize sensing. In this case, the BS only needs to optimize the power allocation of P communication beams, that is, the BS only needs to optimize the power allocation factor $\{\rho_{q,1}^c, \rho_{q,2}^c, \dots, \rho_{q,P}^c\}$, while ρ_q^s is fixed as $\rho_q^s = 0$.
- 2) When Θ_q is located within S4S sectors, the BS needs to optimize P communications beams and one sensing beam simultaneously to maximize the sensing performance while ensuring communications performance. That is, the BS needs to optimize the power allocation factor $\{\rho_q^s, \rho_{q,1}^c, \rho_{q,2}^c, \dots, \rho_{q,P}^c\}$.

The difficulty of the above design is that the interference of rotating sensing beam on communications beams is dynamically changing during SBS stage. Therefore, BS must carefully and quickly update power allocation factor for each time slot to suppress interference, which will be addressed in Section III.

D. Clutter Environment

Note that the receiving array will receive both the effective echoes caused by interested dynamic targets (dynamic target echoes) and the undesired echoes caused by uninterested background environment. In radar systems, these undesired echoes are usually referred to as “clutter”, including ground clutter, sea clutter, weather clutter, birds clutter, etc [28], [29]. The key difference between dynamic target echoes and clutter lies in their different Doppler frequencies. That is, the Doppler frequency of dynamic target echoes is usually much higher than that of clutter, while the Doppler frequency of clutter is usually zero or a small non-zero value. Specifically, the ground clutter is usually caused by static environment, such as land, mountains, roads, and buildings, etc, and its signal power intensity is usually much higher than that of the dynamic

²This paper takes ϑ_{3dB}^p as a typical value for the width of the C4S sector, which can be adjusted according to actual performance in practical systems.

$$\begin{aligned}
y_{n,m}^{c,p^*,q} &= \mathbf{h}_{c,p^*,n,m}^H \mathbf{x}_{q,n,m} + n_{n,m}^{c,p^*,q} = \gamma_{p^*}' \left[\sum_{p=1}^P \sqrt{\frac{\rho_{q,p}^c P_t}{N_T}} F_{TX}(\vartheta_{p^*}, \vartheta_p) s_{n,m}^{c,p,q} + \sqrt{\frac{\rho_q^s P_t}{N_T}} F_{TX}(\vartheta_{p^*}, \Theta_q) s_{n,m}^{s,q} \right] + n_{n,m}^{c,p^*,q} \\
&= \underbrace{\gamma_{p^*}' \sqrt{\rho_{q,p^*}^c P_t N_T} s_{n,m}^{c,p^*,q}}_{\text{ER}} + \underbrace{\gamma_{p^*}' \sum_{p=1, p \neq p^*}^P \sqrt{\frac{\rho_{q,p}^c P_t}{N_T}} F_{TX}(\vartheta_{p^*}, \vartheta_p) s_{n,m}^{c,p,q}}_{\text{MUI}} + \underbrace{\gamma_{p^*}' \sqrt{\frac{\rho_q^s P_t}{N_T}} F_{TX}(\vartheta_{p^*}, \Theta_q) s_{n,m}^{s,q}}_{\text{SI}} + \underbrace{n_{n,m}^{c,p^*,q}}_{\text{Noise}}. \tag{5}
\end{aligned}$$

target echo, but its Doppler frequency is almost zero [30], [31]. Hence a practical modeling of echo signals should include both dynamic targets echoes and static environment echoes, and BS needs to accurately detect the dynamic targets and estimate their parameters under clutter environment. However, most existing ISAC works [15]–[19] ignore the interference caused by static environmental clutter on dynamic target sensing, which does not match the real scenarios. We will construct a practical ISAC scene with clutter environment and provide a complete dynamic targets sensing scheme in Section IV.

III. JOINT COMMUNICATIONS AND SENSING POWER ALLOCATION OPTIMIZATION

In this section, we will jointly optimize ISAC power allocation for each time slot.

A. Communications Performance Metric

Let us first describe the communications process. The communications channel of the p -th user on the m -th subcarrier of the n -th OFDM symbol can be represented as

$$\mathbf{h}_{c,p,n,m} = \gamma_p e^{-j2\pi f_m \frac{R_p}{c}} \mathbf{a}_{TX}(\vartheta_p) \in \mathbb{C}^{N_T \times 1}, \tag{4}$$

where $\gamma_p = \sqrt{\frac{\lambda^2}{(4\pi R_p)^2}}$ is the channel fading for the p -th user. Then the received communications signal of the p^* -th user on the m -th subcarrier of the n -th symbol in the q -th time slot is $y_{n,m}^{c,p^*,q}$, which is expressed as (5) at the top of this page, where $\gamma_{p^*}' \triangleq \gamma_{p^*} e^{j2\pi f_m \frac{R_{p^*}}{c}}$, $n_{n,m}^{c,p^*,q}$ is the zero-mean additive complex Gaussian white noise at the user with variance σ_{c,p^*}^2 , and $F_{TX}(\theta_1, \theta_2) \triangleq \mathbf{a}_{TX}^H(\theta_1) \mathbf{a}_{TX}(\theta_2)$.

Eq. (5) indicates that the received communications signal is composed of four parts: effective reception (ER), multiple users interference (MUI), sensing interference (SI), and noise (Noise). Note that the sensing beam has a negative interfering effect on the communications beams, and thus the signal-to-interference-plus-noise ratio (SINR) should be used to describe the communications performance. Specifically, the SINR for the p^* -th user in the q -th time slot is

$$\begin{aligned}
\text{SINR}_{c,p^*,q} &= \frac{\mathbb{E}\{|\text{ER}|^2\}}{\mathbb{E}\{|\text{MUI}|^2\} + \mathbb{E}\{|\text{SI}|^2\} + \mathbb{E}\{|\text{Noise}|^2\}} \\
&= \frac{\rho_{q,p^*}^c N_T^2}{\sum_{p=1, p \neq p^*}^P \rho_{q,p}^c G_{TX}(\vartheta_{p^*}, \vartheta_p) + \rho_q^s G_{TX}(\vartheta_{p^*}, \Theta_q) + \frac{N_T \sigma_{c,p^*}^2}{P_t \gamma_{p^*}^2}}, \tag{6}
\end{aligned}$$

where $\mathbb{E}\{\cdot\}$ is the mathematical expectation operator and $G_{TX}(\theta_1, \theta_2)$ is defined as

$$G_{TX}(\theta_1, \theta_2) = |F_{TX}(\theta_1, \theta_2)|^2 = \frac{|\sin[\frac{\pi df_0}{c}(\sin\theta_1 - \sin\theta_2)N_T]|^2}{|\sin[\frac{\pi df_0}{c}(\sin\theta_1 - \sin\theta_2)]|^2}. \tag{7}$$

B. Sensing Performance Metric

The existing ISAC waveform optimization studies usually adopt the signal-to-noise ratio (SNR) of echo signals, and Cramer-Rao lower bound (CRLB), etc, as the sensing performance metric. These indicators are directly related to the target's parameters information. However, in SBS stage, when the BS scans the angle direction Θ_q , it is not known beforehand whether there is a target in this direction and the specific parameters of the target. Hence these indicators mentioned above are not applicable to SBS stage.

Note that when the BS needs to scan the sensing angle direction Θ_q , the potential sensing performance will improve with the increase of *equivalent transmission power* in the Θ_q direction, where the equivalent transmission power couples the actual transmission power, the array gain of the transmitting array, and the array gain of the receiving array. We refer to the equivalent transmission power in the Θ_q direction as the *equivalent sensing power (ESP)* in the q -th time slot, which can be denoted as

$$\check{P}_{s,q} = \mathbb{E}\{|\mathbf{w}_{RX,q}^H \mathbf{a}_{RX}(\Theta_q) \mathbf{a}_{TX}^H(\Theta_q) \mathbf{x}_{q,n,m}|^2\}. \tag{8}$$

Eq. (8) indicates that ESP directly couples the design of power allocation factors, and it effectively couples the design of antenna array pattern. Furthermore, it should be pointed out that ESP used in this work and the sensing performance indicators used in [32] and [33] are essentially consistent.

By submitting (1) into (8), the ESP can be rewritten as

$$\check{P}_{s,q} = \underbrace{\sum_{p=1}^P \frac{\rho_{q,p}^c P_t N_R G_{TX}(\Theta_q, \vartheta_p)}{N_T}}_{\text{CBE-ESP}} + \underbrace{\rho_q^s P_t N_T N_R}_{\text{SBE-ESP}}, \tag{9}$$

where CBE-ESP is the ESP contributed by P communications beams, while SBE-ESP is the ESP contributed by the single sensing beam. Both the CBE-ESP and SBE-ESP are beneficial for sensing and can be utilized by BS for sensing.

C. Joint Communications and Sensing Power Allocation

As described in Section II. C, when the sensing scanning angle Θ_q is located within the $p^\#$ -th C4S sector, BS no longer

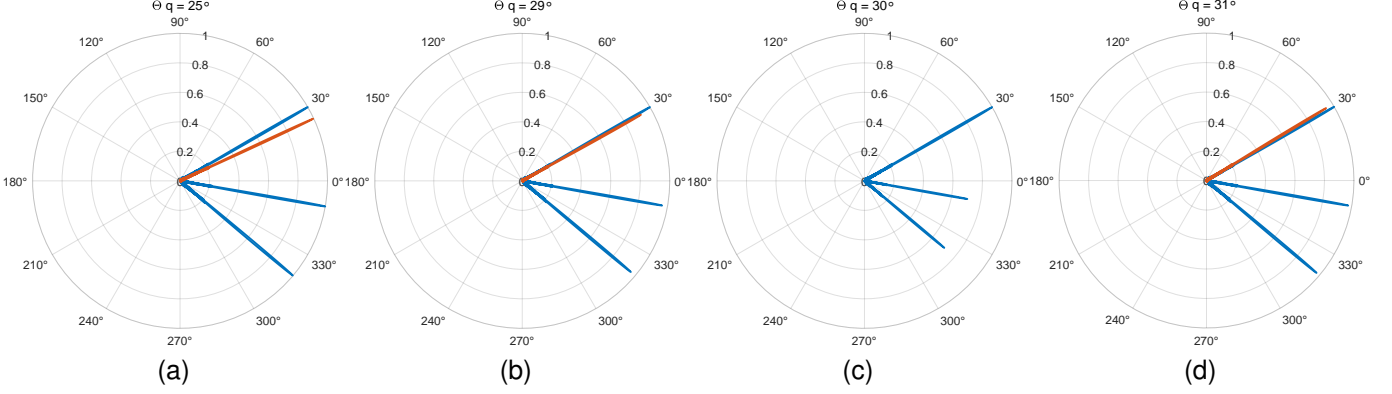


Fig. 5. (a) An example of beamforming optimization results, where Θ_q is 25° . (b) $\Theta_q = 29^\circ$. (c) $\Theta_q = 30^\circ$. (d) $\Theta_q = 31^\circ$. Three users are located in the directions of -40° , -10° , and 30° , respectively. The blue and red lines represent the communications beams and sensing beam, respectively.

generates the dedicated sensing beam, which means that we fix ρ_q^s as $\rho_q^s = 0$ at this time. Then in order to maximize system sensing performance while ensure user communications performance, the overall optimization problem should be formulated as

$$(P1) : \max_{\rho_{q,1}^c, \dots, \rho_{q,p^\#}^c, \dots, \rho_{q,P}^c} \check{P}_{s,q}, \quad (10)$$

$$s.t. \quad \text{SINR}_{c,p^*,q} \geq \epsilon_{p^*}, p^* = 1, 2, \dots, P, \quad (11)$$

$$\rho_q^s + \sum_{p=1}^P \rho_{q,p}^c = 1, \quad (12)$$

$$\rho_q^s = 0, \quad (13)$$

$$\rho_{q,p}^c \geq 0, p = 1, 2, \dots, P, \quad (14)$$

where ϵ_{p^*} is the minimum SINR required for the p^* -th user, and $p^\#$ is a fixed value. To equivalently represent (P1), let us define $\boldsymbol{\rho}_{q,p^\#}^{C4S} = [\rho_{q,1}^c, \dots, \rho_{q,p^\#}^c, \dots, \rho_{q,P}^c]^T \in \mathbb{R}^{P \times 1}$, $\mathbf{n}_{q,p^\#}^{C4S} \in \mathbb{R}^{P \times 1}$ with $\mathbf{n}_{q,p^\#}^{C4S}[p] = \epsilon_{p^*} \frac{N_T \sigma_{c,p^*}^2}{P_t \gamma_{p^*}^2}$, $\mathbf{G}_{q,p^\#}^{C4S} \in \mathbb{R}^{P \times P}$ with $\mathbf{G}_{q,p^\#}^{C4S}[p^*, p] = G_{TX}(\vartheta_{p^*}, \vartheta_p) \epsilon_{p^*}$ for $p^* \neq p$, $\mathbf{G}_{q,p^\#}^{C4S}[p^*, p] = -N_T^2$ for $p^* = p$, and $\mathbf{m}_{q,p^\#}^{C4S} \in \mathbb{R}^{P \times 1}$ with $\mathbf{m}_{q,p^\#}^{C4S}[p] = \frac{P_t N_R G_{TX}(\Theta_q, \vartheta_p)}{N_T}$. Then by submitting (6) and (9) into (11) and (10), (P1) can be equivalently transformed as

$$(P1.1) : \maximize_{\boldsymbol{\rho}_{q,p^\#}^{C4S}} (\mathbf{m}_{q,p^\#}^{C4S})^T \boldsymbol{\rho}_{q,p^\#}^{C4S}, \quad (15)$$

$$s.t. \quad \mathbf{G}_{q,p^\#}^{C4S} \boldsymbol{\rho}_{q,p^\#}^{C4S} + \mathbf{n}_{q,p^\#}^{C4S} \leq 0, \quad (16)$$

$$\mathbf{1}^T \boldsymbol{\rho}_{q,p^\#}^{C4S} - 1 = 0, \quad (17)$$

$$\rho_q^s = 0, \quad (18)$$

$$\boldsymbol{\rho}_{q,p^\#}^{C4S} \geq 0. \quad (19)$$

It is seen that (P1.1) is a linear programming (LP) problem, and thus we can directly use CVX to solve it [34], [35].

On the other side, when Θ_q is located within S4S sectors,

the overall optimization problem is formulated into

$$(P2) : \maximize_{\rho_q^s, \rho_{q,1}^c, \dots, \rho_{q,P}^c} \check{P}_{s,q}, \quad (20)$$

$$s.t. \quad \text{SINR}_{c,p^*,q} \geq \epsilon_{p^*}, p^* = 1, 2, \dots, P, \quad (21)$$

$$\rho_q^s + \sum_{p=1}^P \rho_{q,p}^c = 1, \quad (22)$$

$$\rho_q^s \geq 0, \rho_{q,p}^c \geq 0, p = 1, \dots, P. \quad (23)$$

Let us define $\boldsymbol{\rho}_q^{S4S} = [\rho_{q,1}^c, \dots, \rho_{q,P}^c, \rho_q^s]^T \in \mathbb{R}^{(P+1) \times 1}$, $\mathbf{n}_q^{S4S} \in \mathbb{R}^{P \times 1}$ with $\mathbf{n}_q^{S4S}[p] = \epsilon_{p^*} \frac{N_T \sigma_{c,p^*}^2}{P_t \gamma_{p^*}^2}$, $\mathbf{m}_q^{S4S} \in \mathbb{R}^{(P+1) \times 1}$ with $\mathbf{m}_q^{S4S}[p] = \frac{P_t N_R G_{TX}(\Theta_q, \vartheta_p)}{N_T}$ for $p = 1, \dots, P$, $\mathbf{m}_q^{S4S}[P+1] = P_t N_T N_R$, and $\mathbf{G}_q^{S4S} \in \mathbb{R}^{P \times (P+1)}$ with

$$\mathbf{G}_q^{S4S}[p^*, p] = \begin{cases} G_{TX}(\vartheta_{p^*}, \vartheta_p) \epsilon_{p^*}, & \text{if } p^* \neq p, 1 \leq p \leq P \\ -N_T^2, & \text{if } p^* = p, 1 \leq p \leq P \\ G_{TX}(\vartheta_{p^*}, \Theta_q) \epsilon_{p^*}, & \text{if } p = P+1. \end{cases} \quad (24)$$

Then by submitting (6) and (9) into (21) and (20), (P2) can be equivalently transformed into

$$(P2.1) : \max_{\boldsymbol{\rho}_q^{S4S}} (\mathbf{m}_q^{S4S})^T \boldsymbol{\rho}_q^{S4S}, \quad (25)$$

$$s.t. \quad \mathbf{G}_q^{S4S} \boldsymbol{\rho}_q^{S4S} + \mathbf{n}_q^{S4S} \leq 0, \quad (26)$$

$$\mathbf{1}^T \boldsymbol{\rho}_q^{S4S} - 1 = 0, \quad (27)$$

$$\boldsymbol{\rho}_q^{S4S} \geq 0. \quad (28)$$

It can be found that (P2.1) is also an LP problem, and thus we can use CVX to solve it too.

Fig. 5 shows the examples of transmitting beamforming with multiple users, in which $N_T = 128$ antennas are configured and three users are located in -40° , -10° and 30° , respectively. The blue and red lines represent the communications beams and sensing beam, respectively. Fig. 5(a) to Fig. 5(d) show several silhouettes with Θ_q gradually scanning from 25° to 31° , and this process undergoes a C4S sector formed by the user at 30° as $[29.5452^\circ, 30.4548^\circ]$. In Fig. 5(a), due to the difference between $\Theta_q = 25^\circ$ and users angles, an obvious red sensing beam in 25° direction can be observed. In Fig. 5(c), the Θ_q is set as 30° , which is within one C4S sector.

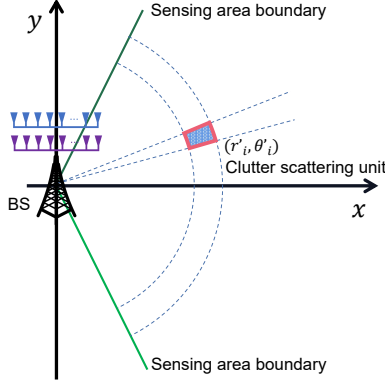


Fig. 6. Schematic diagram of static environmental clutter scattering unit.

Then the optimization result at this time is $\rho_q^s = 0$, which means that BS does not allocate energy to the sensing beam in order to ensure the communications performance of the user in 30° direction. Fortunately, the communications beam focused toward the 30° direction can still be utilized by the BS for sensing at this time.

IV. DYNAMIC TARGET DETECTION AND ESTIMATION IN CLUTTER ENVIRONMENT

In this section, we will construct a practical ISAC scene with clutter environment and provide a complete and practical scheme to sense dynamic targets from clutter environment.

A. Echo Signals Model

As described in Section II. D, the original echo signals should include both dynamic targets echoes (DTE) and static environment echoes (SEE). Based on typical urban service scenarios, we model the clutter environment as ground clutter. Specifically, we divide the clutter area within sensing range into I static clutter scattering units based on distance and angle dimensions as the blue grid unit in Fig. 6, and the size of the clutter scattering unit is determined by the angle and distance resolution of the system. Assuming the center position of the i -th unit is (r'_i, θ'_i) , Then the echo channel of the i -th unit on the m -th subcarrier of the n -th symbol can be modeled as

$$\mathbf{H}'_{i,n,m} = \beta_i e^{-j2\pi f_m \frac{2r'_i}{c}} \mathbf{a}_{RX}(\theta'_i) \mathbf{a}_{TX}^H(\theta'_i), \quad i = 1, \dots, I, \quad (29)$$

where $\beta_i = \sqrt{\frac{\lambda^2}{(4\pi)^3 r_i'^4}} \sigma'_{c,i}$ is the channel fading factor and $\sigma'_{c,i}$ is the radar cross section (RCS) of the i -th clutter scattering unit. The RCS of ground clutter can usually be assumed to follow the Swerling I model, and the probability density function of RCS σ satisfies

$$f(\sigma) = \frac{1}{\sigma_0} \exp\left(-\frac{\sigma}{\sigma_0}\right), \sigma \geq 0, \quad (30)$$

where σ_0 is the average value of object's RCS. Besides, the echo channel of the k -th dynamic target on the m -th subcarrier of the n -th OFDM symbol can be represented as

$$\mathbf{H}_{k,n,m} = \alpha_k e^{j2\pi f_0 \frac{2v_k n T_s}{c}} e^{-j2\pi f_m \frac{2r_k}{c}} \mathbf{a}_{RX}(\theta_k) \mathbf{a}_{TX}^H(\theta_k), \quad (31)$$

$$k = 1, \dots, K,$$

where $n = 0, 1, 2, \dots, N-1$, $\alpha_k = \sqrt{\frac{\lambda^2}{(4\pi)^3 r_k^4}} \sigma_{c,k}$, and $\sigma_{c,k}$ is the RCS of the k -th dynamic target that also follows Swerling I model. Based on (29) and (31), the overall sensing echoes channel matrix on the m -th subcarrier of the n -th OFDM symbol can be represented as

$$\mathbf{H}_{n,m} = \sum_{k=1}^K \mathbf{H}_{k,n,m} + \sum_{i=1}^I \mathbf{H}'_{i,n,m}. \quad (32)$$

Based on (1) and (32), the echo signal on the m -th subcarrier of the n -th OFDM symbol received by BS in the q -th time slot is

$$y_{n,m}^{s,q} = \mathbf{w}_{RX,q}^H \mathbf{H}_{n,m} \mathbf{x}_{q,n,m} + n_{n,m}^{s,q}$$

$$= \sum_{p=1}^P \mathbf{w}_{RX,q}^H \mathbf{H}_{n,m} \mathbf{w}_{c,p,q} s_{n,m}^{c,p,q} + \mathbf{w}_{RX,q}^H \mathbf{H}_{n,m} \mathbf{w}_{s,q} s_{n,m}^{s,q} + n_{n,m}^{s,q},$$

$$q = 1, \dots, Q, \quad n = 0, \dots, N-1, \quad m = 0, \dots, M-1, \quad (33)$$

where $n_{n,m}^{s,q}$ is the zero-mean additive Gaussian noise with variance $\sigma_{s,q}^2$. Then we can stack $y_{n,m}^{s,q}$ into one echoes tensor $\mathbf{Y}_{cube} \in \mathbb{C}^{Q \times N \times M}$, whose (q, n, m) -th element is $\mathbf{Y}_{cube}[q, n, m] = y_{n,m}^{s,q}$.

Note that \mathbf{Y}_{cube} includes the echoes channel, receiving and transmitting beamforming, and transmission symbols, while targets sensing can be understood as an estimation of echoes channel. However, random transmission symbols would affect the estimation of echoes channel, and thus we need to erase the transmission symbols from the received signals to obtain the equivalent echoes channel (EEC) [19]. For massive MIMO system, when Θ_q is located within the S4S sector, it can be inferred from (33) that $y_{n,m}^{s,q} \approx \mathbf{w}_{RX,q}^H \mathbf{H}_{n,m} \mathbf{w}_{s,q} s_{n,m}^{s,q} + n_{n,m}^{s,q}$, which means that the sensing echoes are mainly provided by the sensing beam at this time, and thus the EEC corresponding to $y_{n,m}^{s,q}$ can be obtained as $\tilde{h}_{n,m}^{s,q} = y_{n,m}^{s,q} / s_{n,m}^{s,q}$. When Θ_q is located within the p -th C4S sector, it can be inferred from (33) that $y_{n,m}^{s,q} \approx \mathbf{w}_{RX,q}^H \mathbf{H}_{n,m} \mathbf{w}_{c,p,q} s_{n,m}^{c,p,q} + n_{n,m}^{s,q}$, which means that the sensing echoes are mainly provided by the p -th communications beam at this time, and thus the EEC corresponding to $y_{n,m}^{s,q}$ can be obtained as $\tilde{h}_{n,m}^{s,q} = y_{n,m}^{s,q} / s_{n,m}^{c,p,q}$. Then we can comprehensively define the EEC as $\tilde{h}_{n,m}^{s,q} = y_{n,m}^{s,q} / s_{n,m}^{t,q}$, where $s_{n,m}^{t,q}$ is designed as

$$s_{n,m}^{t,q} = \begin{cases} s_{n,m}^{s,q}, & \text{if } \Theta_q \notin \left(\vartheta_p - \frac{\vartheta_p^p}{2}, \vartheta_p + \frac{\vartheta_p^p}{2}\right) \text{ for all } p = 1, \dots, P; \\ s_{n,m}^{c,p,q}, & \text{if } \Theta_q \in \left[\vartheta_p - \frac{\vartheta_p^p}{2}, \vartheta_p + \frac{\vartheta_p^p}{2}\right] \text{ for any } p = 1, \dots, P. \end{cases} \quad (34)$$

Besides, we can stack $\tilde{h}_{n,m}^{s,q}$ into an EEC tensor $\tilde{\mathbf{H}}_{cube} \in \mathbb{C}^{Q \times N \times M}$, with $\tilde{\mathbf{H}}_{cube}[q, n, m] = \tilde{h}_{n,m}^{s,q}$.

B. Static Environmental Clutter Filtering

It can be analyzed from (32) and (33) that the echo signals \mathbf{Y}_{cube} includes both DTE and SEE, and the corresponding EEC $\tilde{\mathbf{H}}_{cube}$ also includes both the EEC of dynamic targets (DT-EEC) and the EEC of static environment (SE-EEC). As introduced in Section I, the sensing tasks of ISAC system can

be divided into SES and DTS, while DTS can be considered as an estimation of DT-EEC. However, when we focus on DTS problem, the SE-EEC in the original echo signals would cause negative interference to DTS, and thus SE-EEC can be referred to as the clutter-EEC. To address this negative interference, we need to filter out the interference of clutter-EEC (SE-EEC) and to extract the effective DT-EEC from $\tilde{\mathbf{H}}_{cube}$.

To begin with, the EEC of the m -th subcarrier in $\tilde{\mathbf{H}}_{cube}$ can be denoted as $\tilde{\mathbf{H}}_m^M = \tilde{\mathbf{H}}_{cube}[:, :, m] \in \mathbb{C}^{Q \times N}$, i.e.,

$$\tilde{\mathbf{H}}_m^M = \begin{bmatrix} \mathbf{w}_{RX,1}^H \mathbf{H}_{0,m} \tilde{\mathbf{x}}_{1,0,m} & \cdots & \mathbf{w}_{RX,1}^H \mathbf{H}_{N-1,m} \tilde{\mathbf{x}}_{1,N-1,m} \\ \vdots & \ddots & \vdots \\ \mathbf{w}_{RX,Q}^H \mathbf{H}_{0,m} \tilde{\mathbf{x}}_{Q,0,m} & \cdots & \mathbf{w}_{RX,Q}^H \mathbf{H}_{N-1,m} \tilde{\mathbf{x}}_{Q,N-1,m} \end{bmatrix} + \mathbf{N}_m^M \quad (35)$$

where $\tilde{\mathbf{x}}_{q,n,m} = \mathbf{x}_{q,n,m}/s_{n,m}^{t,q}$, and the (q,n) -th element in \mathbf{N}_m^M is $\mathbf{N}_m^M[q,n] = n_{n,m}^{s,q}/s_{n,m}^{t,q}$. Clearly, $\tilde{\mathbf{H}}_m^M$ includes both SE-EEC and DT-EEC. The idea is to first calculate the SE-EEC as $\tilde{\mathbf{H}}_m^{static}$, and then subtract $\tilde{\mathbf{H}}_m^{static}$ from the total channel $\tilde{\mathbf{H}}_m^M$ to obtain the DT-EEC as $\tilde{\mathbf{H}}_m^{dynamic} = \tilde{\mathbf{H}}_m^M - \tilde{\mathbf{H}}_m^{static}$.

Specifically, considering that the phase of SE-EEC remains unchanged within multiple OFDM symbols, while the phase of DT-EEC changes linearly with the target velocity within multiple OFDM symbols, we may average each row of $\tilde{\mathbf{H}}_m^M$ and obtain the equivalent echoes channel vector caused by static environment as $\tilde{\mathbf{h}}_m^{static} \in \mathbb{C}^{Q \times 1}$, whose q -th element is

$$\begin{aligned} \tilde{h}_m^{static}[q] &= \tilde{h}_{m,q}^{static} = \frac{1}{N} \sum_{n=0}^{N-1} \tilde{h}_{n,m}^{s,q} = \frac{1}{N} \sum_{n=0}^{N-1} y_{n,m}^{s,q}/s_{n,m}^{t,q} \\ &\approx \mathbf{w}_{RX,q}^H \left(\sum_{i=1}^I \mathbf{H}'_{i,n,m} \right) \tilde{\mathbf{x}}_{q,n,m} + \tilde{n}_{m,q}^{static}. \end{aligned} \quad (36)$$

The detailed derivation of (36) can be found in Appendix A. Eq. (36) indicates that the average of $\tilde{h}_{n,m}^{s,q}$ for fixed m and q can be used to express the static clutter channel. Then the $\tilde{\mathbf{h}}_m^{static}$ can be used to reconstruct the SE-EEC as $\tilde{\mathbf{H}}_m^{static} = [\tilde{h}_m^{static}, \dots, \tilde{h}_m^{static}] \in \mathbb{C}^{Q \times N}$. Then the DT-EEC of the m -th subcarrier can be extracted as $\tilde{\mathbf{H}}_m^{dynamic} = \tilde{\mathbf{H}}_m^M - \tilde{\mathbf{H}}_m^{static}$, and

we represent the (q,n) -th element in $\tilde{\mathbf{H}}_m^{dynamic}$ as

$$\begin{aligned} \check{h}_{q,n,m} &= \mathbf{w}_{RX,q}^H \left(\sum_{k=1}^K \mathbf{H}_{k,n,m} \right) \tilde{\mathbf{x}}_{q,n,m} \\ &\quad - \underbrace{\frac{1}{N} \sum_{n=0}^{N-1} \left[\mathbf{w}_{RX,q}^H \left(\sum_{k=1}^K \mathbf{H}_{k,n,m} \right) \tilde{\mathbf{x}}_{q,n,m} \right]}_{\mathcal{I}'_{q,n,m}} + \check{n}_{n,m}^{s,q}, \end{aligned} \quad (37)$$

where $\mathcal{I}'_{q,n,m}$ is defined as the remaining term after clutter filtering, and $\check{n}_{n,m}^{s,q} = n_{n,m}^{s,q}/s_{n,m}^{t,q} - \frac{1}{N} \sum_{n=0}^{N-1} n_{n,m}^{s,q}/s_{n,m}^{t,q}$. Because the Doppler term in DT-EEC varies linearly with continuous symbols, according to the derivation process in Appendix A, there is $\lim_{N \rightarrow \infty} \mathcal{I}'_{q,n,m} = 0$. Thus we have eliminated the influence of static environmental clutter.

After filtering out the static environmental clutter, the $\check{h}_{q,n,m}$ in (37) can be rewritten as (38) at the bottom of this page, where $e^{j\phi_{n,m}^{k,q}} = e^{j\frac{4\pi f_0 v_k n T_s}{c}} e^{-j\frac{4\pi f_m r_k}{c}}$, and $F_{RX}(\theta_1, \theta_2) \triangleq \mathbf{a}_{RX}^H(\theta_1) \mathbf{a}_{RX}(\theta_2)$. Considering the randomness of dynamic target distribution, we assume that there are K_q dynamic targets simultaneously in the direction Θ_q with $\sum_{q=1}^Q K_q = K$. For massive MIMO systems with $N_T \rightarrow \infty$ and $N_R \rightarrow \infty$, $\check{h}_{q,n,m}$ can be further calculated as (39) at the bottom of this page. Then the $\check{h}_{q,n,m}$ on all subcarriers of all OFDM symbols in all time slots can be stacked into a DT-EEC tensor $\tilde{\mathbf{H}}_{cube}^{dynamic} \in \mathbb{C}^{Q \times N \times M}$, whose (q,n,m) -th element is $\tilde{\mathbf{H}}_{cube}^{dynamic}[q,n,m] = \check{h}_{q,n,m}$.

C. Dynamic Targets Detection and Angle Estimation

In order to detect the presence of dynamic targets from $\tilde{\mathbf{H}}_{cube}^{dynamic}$, we extract the DT-EEC of the m -th subcarrier from $\tilde{\mathbf{H}}_{cube}^{dynamic}$ as $\tilde{\mathbf{H}}_m^{dynamic} = \tilde{\mathbf{H}}_{cube}^{dynamic}[:, :, m] \in \mathbb{C}^{Q \times N}$. Next, considering that the sensing scanning angle dimension in $\tilde{\mathbf{H}}_m^{dynamic}$ contains angle information of dynamic targets while the OFDM symbol dimension contains velocity information of dynamic targets, we perform an N -point fast fourier transform (FFT) on each row of $\tilde{\mathbf{H}}_m^{dynamic}$, and move the zero-frequency component of the transformed spectrum to the center of the array [36], [37]. By doing so, we can obtain the angle-Doppler spectrum for DT-EEC of the m -th subcarrier as

$$\tilde{\mathbf{H}}_m^{AD} = \text{FFTshift}\{\text{FFT}\{\tilde{\mathbf{H}}_m^{dynamic}, N, 2\}, N, 2\}, \quad (40)$$

where $\text{FFT}\{\tilde{\mathbf{H}}_m^{dynamic}, N, 2\}$ refers to performing N -point FFT on each row of $\tilde{\mathbf{H}}_m^{dynamic}$, and $\text{FFTshift}\{\mathbf{A}, N, 2\}$ refers

$$\begin{aligned} \check{h}_{q,n,m} &= \tilde{\mathbf{H}}_m^{dynamic}[q,n] \approx \mathbf{w}_{RX,q}^H \left(\sum_{k=1}^K \mathbf{H}_{k,n,m} \right) \tilde{\mathbf{x}}_{q,n,m} + \check{n}_{n,m}^{s,q} \\ &= \sum_{k=1}^K \left\{ \frac{\alpha_k e^{j\phi_{n,m}^{k,q}}}{\sqrt{N_R}} F_{RX}(\Theta_q, \theta_k) \left[\sum_{p=1}^P \sqrt{\frac{\rho_{q,p}^c P_t}{N_T}} F_{TX}(\theta_k, \vartheta_p) \frac{s_{n,m}^{c,p,q}}{s_{n,m}^{t,q}} + \sqrt{\frac{\rho_q^s P_t}{N_T}} F_{TX}(\theta_k, \Theta_q) \frac{s_{n,m}^{s,q}}{s_{n,m}^{t,q}} \right] \right\} + \check{n}_{n,m}^{s,q}, \end{aligned} \quad (38)$$

$$\check{h}_{q,n,m} \approx \begin{cases} \check{n}_{n,m}^{s,q}, & \text{if } \Theta_q \neq \theta_k \text{ for all } k = 1, \dots, K, \\ \sum_{k'=1}^{K_q} \alpha_{k'} e^{j\phi_{n,m}^{k',q}} \sqrt{\rho_{q,t}^s P_t N_T N_R} + \check{n}_{n,m}^{s,q}, & \text{if } \Theta_q = \theta_k \neq \vartheta_p \text{ for part of } k \text{ and for all } p = 1, \dots, P, \\ \sum_{k'=1}^{K_q} \alpha_{k'} e^{j\phi_{n,m}^{k',q}} \sqrt{\rho_{q,p}^c P_t N_T N_R} + \check{n}_{n,m}^{s,q}, & \text{if } \Theta_q = \theta_k = \vartheta_p \text{ for part of } k \text{ and any } p = 1, \dots, P. \end{cases} \quad (39)$$

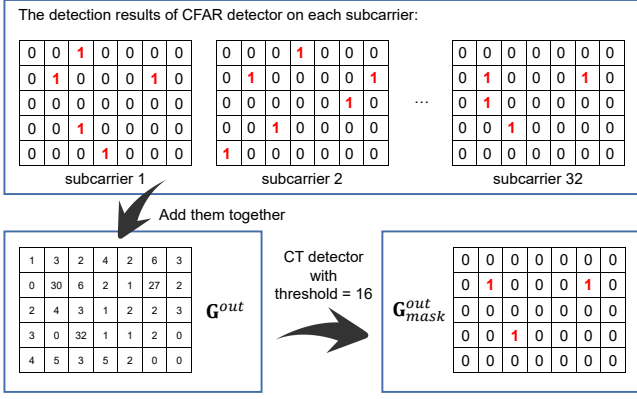


Fig. 7. A simple schematic diagram of the proposed MSJD algorithm, where the number of subcarriers is $M = 32$. The horizontal and vertical axes of the matrix represent angle units and velocity units, respectively.

to performing N -point spectral centralization on each row of \mathbf{A} . For clarity, we introduce a corresponding matrix $\tilde{\mathbf{G}}_m^{AD}$ for $\tilde{\mathbf{H}}_m^{AD}$, which satisfies $\tilde{\mathbf{G}}_m^{AD}[q, n] = |\tilde{\mathbf{H}}_m^{AD}[q, n]|$. It can be analyzed from (39) that when the resolutions of angle and velocity are sufficient, there will be K peaks in $\tilde{\mathbf{G}}_m^{AD}$, which correspond to K dynamic targets one by one.

To further overcome the impact of noise and other factors, it is necessary to set appropriate local thresholds to detect each target from $\tilde{\mathbf{G}}_m^{AD}$, which is referred to as *radar target detection*. Constant threshold (CT) detector and constant false alarm rate (CFAR) detector are two main methods for target detection³ [38]. Here, we propose a joint detection method over multiple subcarriers (MSJD) based on CFAR and CT detectors, which can be divided into the following two steps: 1) We take $\tilde{\mathbf{G}}_m^{AD}$ as the input, set appropriate reference range and protection range, and perform two-dimensional cell-averaging CFAR (2D-CA-CFAR) detection on $\tilde{\mathbf{G}}_m^{AD}$. Then we can obtain the judgment matrix over single subcarrier \mathbf{G}_m^{out} as the output. 2) We compute \mathbf{G}_m^{out} for each subcarrier, and accumulate them together to obtain $\mathbf{G}^{out} = \sum_{m=1}^M \mathbf{G}_m^{out}$. Next we set a fixed threshold and perform CT detection on \mathbf{G}^{out} to obtain the judgment matrix over multiple subcarriers as \mathbf{G}_{mask}^{out} . Then we can detect each target from \mathbf{G}_{mask}^{out} , and the accurate angle estimation results for each dynamic target can also be obtained from \mathbf{G}_{mask}^{out} as $\{\hat{\theta}_1, \hat{\theta}_2, \dots, \hat{\theta}_K\}$. For clarity, Fig. 7 shows a simple application example of the proposed MSJD algorithm.

Fig. 8 shows examples of clutter filtering, angle-Doppler spectrum estimation (ADSE) and MSJD under noiseless conditions, where five dynamic targets are set as $(100m, -40^\circ, 10m/s)$, $(60m, -10^\circ, 5m/s)$, $(90m, 30^\circ, 15m/s)$, $(150m, 30^\circ, -10m/s)$ and $(200m, 30^\circ, -25m/s)$. It is seen from Fig. 8(a) that the original echo signals carry dense clutter caused by

³The problem of radar target detection is to use the statistical characteristics of signals and noise or clutter to solve the decision problem of whether the target signal is present or not. CFAR detector aims to detect the targets in echo signals with a constant false alarm rate, that is, to accurately identify the presence of targets as much as possible while maintaining a low false alarm rate. For this effect, CFAR adaptively adjusting the detection threshold to maintain the false alarm rate, and it can adapt to different environments with different levels of background noise.

static environment. After clutter filtering, Fig. 8(b) only retains the effective echoes caused by dynamic targets. After performing velocity FFT on the complex signals, five peaks corresponding to five dynamic targets can be clearly observed in the angle-Doppler spectrum shown in Fig. 8(c), which can also be observed in the MSJD results shown in Fig. 8(d). Then the angle estimates of the dynamic targets can be obtained as -40° , -10° , 30° , 30° and 30° , respectively.

D. Distance and Velocity Estimation for Dynamic Targets

After obtaining angle estimates, we may suppose that K_q detected targets are located in the same angle Θ_q , and represent the parameters of the k'_q -th dynamic target as $(r_{k'_q}, \Theta_q, v_{k'_q})$, where $k'_q = 1, 2, \dots, K_q$. Then the DT-EEC of this beam scanning angle within all subcarriers and symbols can be represented as $\tilde{\mathbf{H}}_q^{RD} \in \mathbb{C}^{N \times M}$, whose (n, m) -th element is $\tilde{\mathbf{H}}_q^{RD}[n, m] = \tilde{h}_{q,n,m}$. Based on (39), $\tilde{\mathbf{H}}_q^{RD}$ and its transpose matrix $(\tilde{\mathbf{H}}_q^{RD})^T$ can be respectively represented as

$$\tilde{\mathbf{H}}_q^{RD} = \zeta_q \sum_{k'_q=1}^{K_q} \alpha'_{k'_q} \mathbf{k}_D(v_{k'_q}) \mathbf{k}_R^T(r_{k'_q}) + \mathbf{N}_q^{RD}, \quad (41)$$

$$(\tilde{\mathbf{H}}_q^{RD})^T = \zeta_q \sum_{k'_q=1}^{K_q} \alpha'_{k'_q} \mathbf{k}_R(r_{k'_q}) \mathbf{k}_D^T(v_{k'_q}) + (\mathbf{N}_q^{RD})^T, \quad (42)$$

where ζ_q is the amplitude term, $\alpha'_{k'_q} = \alpha_{k'_q} e^{-j \frac{4\pi f_0 r_{k'_q}}{c}}$, \mathbf{N}_q^{RD} is the corresponding noise matrix, $\mathbf{k}_D(v) = [1, e^{j \frac{4\pi f_0 v T_s}{c}}, \dots, e^{j \frac{4\pi f_0 v T_s (N-1)}{c}}]^T \in \mathbb{C}^{N \times 1}$ is defined as the *Doppler array steering vector*, and $\mathbf{k}_R(r) = [1, e^{-j \frac{4\pi r \Delta f}{c}}, \dots, e^{-j \frac{4\pi r \Delta f (M-1)}{c}}]^T \in \mathbb{C}^{M \times 1}$ is defined as the *distance array steering vector*. From (40) and (41), it can be seen that $\tilde{\mathbf{H}}_q^{RD}$ and $(\tilde{\mathbf{H}}_q^{RD})^T$ are the generalized array signals related to Doppler array and distance array, respectively. To estimate the velocity and distance of dynamic targets, the autocorrelation matrices of $\tilde{\mathbf{H}}_q^{RD}$ and $(\tilde{\mathbf{H}}_q^{RD})^T$ are calculated as $\mathbf{R}_{D,q}^X = \frac{1}{M} \tilde{\mathbf{H}}_q^{RD} (\tilde{\mathbf{H}}_q^{RD})^H$ and $\mathbf{R}_{R,q}^X = \frac{1}{N} (\tilde{\mathbf{H}}_q^{RD})^T ((\tilde{\mathbf{H}}_q^{RD})^T)^H$. We perform eigenvalue decomposition of $\mathbf{R}_{D,q}^X$ and $\mathbf{R}_{R,q}^X$ to obtain the diagonal matrix with eigenvalues ranging from large to small ($\Sigma_{D,q}$ and $\Sigma_{R,q}$) and the corresponding eigenvector matrix ($\mathbf{U}_{D,q}$ and $\mathbf{U}_{R,q}$). That is $[\mathbf{U}_{D,q}, \Sigma_{D,q}] = \text{eig}(\mathbf{R}_{D,q}^X)$ and $[\mathbf{U}_{R,q}, \Sigma_{R,q}] = \text{eig}(\mathbf{R}_{R,q}^X)$. Then the minimum description length (MDL) criterion is utilized to estimate the number of dynamic targets from $\Sigma_{D,q}$ and $\Sigma_{R,q}$ as $K_{q,D}^{MDL}$ and $K_{q,R}^{MDL}$ respectively [39], [40], and we define $K_q^{MDL} = \min\{K_{q,D}^{MDL}, K_{q,R}^{MDL}\}$ as the number of dynamic targets to be estimated from \mathbf{H}_q^{RD} . Therefore, the noise space related to the Doppler array can be represented as $\mathbf{U}_{D,q}^N = \mathbf{U}_{D,q}[:, K_q^{MDL} + 1 : N]$, and the noise space related to the distance array can be represented as $\mathbf{U}_{R,q}^N = \mathbf{U}_{R,q}[:, K_q^{MDL} + 1 : M]$. Then the Doppler spectral function with search velocity v and the distance spectral function with search distance r can be defined as

$$F_{D,q}(v) = \frac{1}{\mathbf{k}_D^H(v) \mathbf{U}_{D,q}^N (\mathbf{U}_{D,q}^N)^H \mathbf{k}_D(v)}, \quad (43)$$

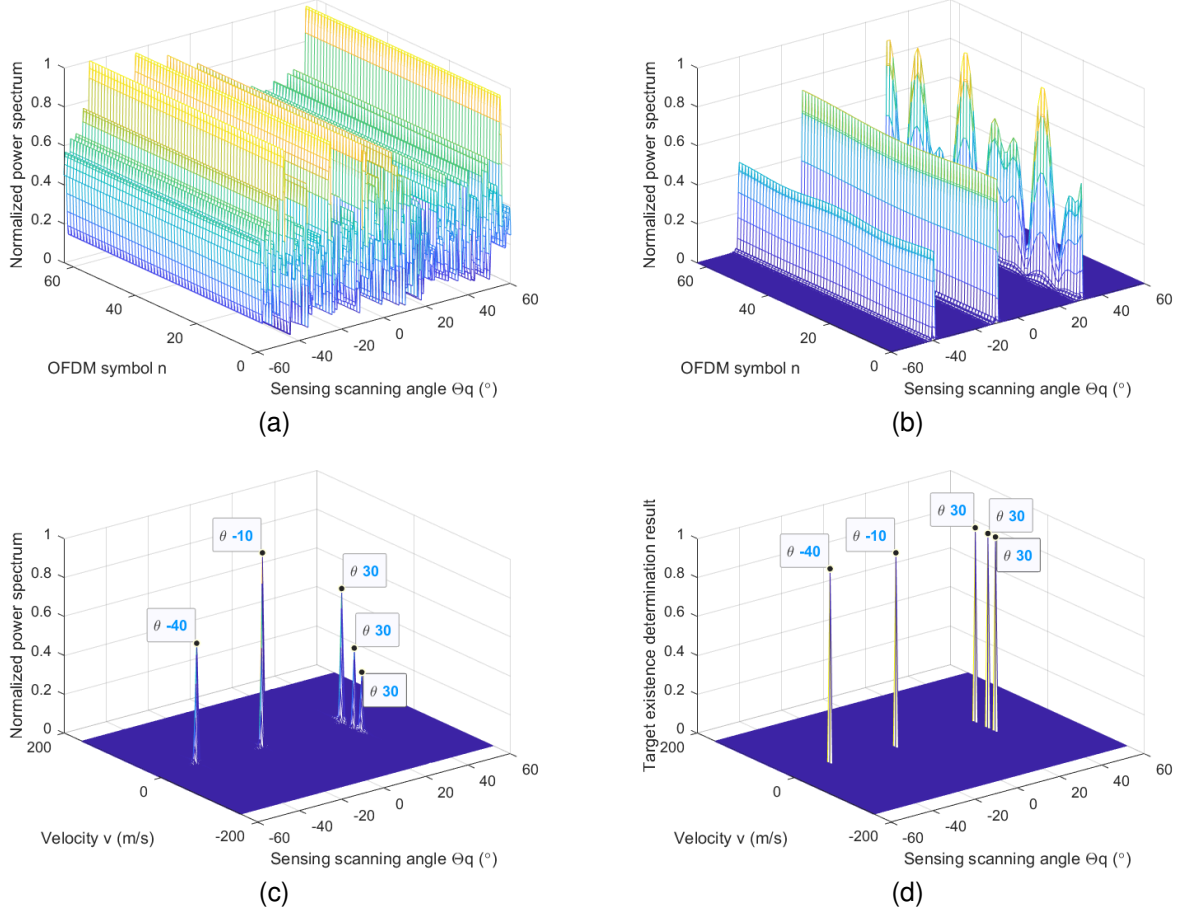
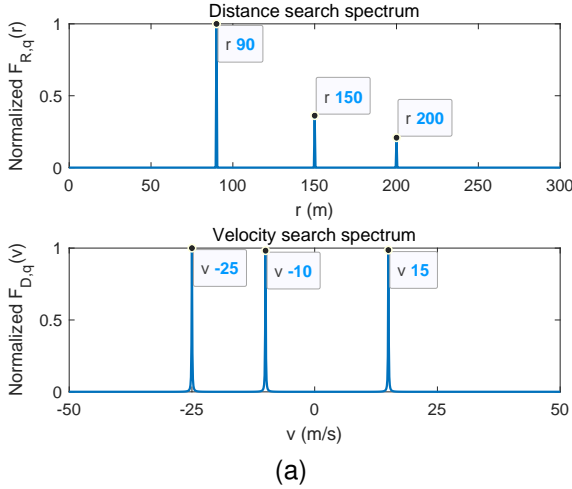


Fig. 8. (a) The power spectrum of the original echo signals on a certain subcarrier. (b) Signal power spectrum after filtering out static environmental clutter. (c) The angle-Doppler spectrum. (d) The detection results of MSJD. The five dynamic targets are set as $(100m, -40^{\circ}, 10m/s)$, $(60m, -10^{\circ}, 5m/s)$, $(90m, 30^{\circ}, 15m/s)$, $(150m, 30^{\circ}, -10m/s)$ and $(200m, 30^{\circ}, -25m/s)$.



Distance-Velocity Matching

$$\check{r}_1 = 90m, \check{r}_2 = 150m, \check{r}_3 = 200m$$

$$\check{v}_1 = -25m/s, \check{v}_2 = -10m/s, \check{v}_3 = 15m/s$$

Results after matching

$$(\hat{r}_{30^{\circ},1}, \hat{v}_{30^{\circ},1}) = (\check{r}_1, \check{v}_3) = (90m, 15m/s)$$

$$(\hat{r}_{30^{\circ},2}, \hat{v}_{30^{\circ},2}) = (\check{r}_2, \check{v}_2) = (150m, -10m/s)$$

$$(\hat{r}_{30^{\circ},3}, \hat{v}_{30^{\circ},3}) = (\check{r}_3, \check{v}_1) = (200m, -25m/s)$$

\check{r}_i	\check{v}_j	Normalized $S_q(\check{r}_i, \check{v}_j)$
\check{r}_1	\check{v}_1	0.022
\check{r}_1	\check{v}_2	0.021
\check{r}_1	\check{v}_3	1.000
\check{r}_2	\check{v}_1	0.021
\check{r}_2	\check{v}_2	0.600
\check{r}_2	\check{v}_3	0.014
\check{v}_3	\check{v}_1	0.450
\check{v}_3	\check{v}_2	0.020
\check{v}_3	\check{v}_3	0.009

Fig. 9. (a) An example of velocity estimation based on searching $F_{D,q}(v)$; (b) An example of distance estimation based on searching $F_{R,q}(r)$. Three dynamic targets are set as $(90m, 30^{\circ}, 15m/s)$, $(150m, 30^{\circ}, -10m/s)$ and $(200m, 30^{\circ}, -25m/s)$.

$$F_{R,q}(r) = \frac{1}{\mathbf{k}_R^H(r) \mathbf{U}_{R,q}^N (\mathbf{U}_{R,q}^N)^H \mathbf{k}_R(r)}. \quad (44)$$

By searching for the peaks of $F_{D,q}(v)$ and $F_{R,q}(r)$, we can obtain the preliminary velocity estimates for K_q targets as $\{\check{v}_1, \check{v}_2, \dots, \check{v}_{K_q}\}$ and the preliminary distance estimates for

K_q targets as $\{\check{r}_1, \check{r}_2, \dots, \check{r}_{K_q}\}$, respectively. Next, in order to obtain the unique parameters information for each target from the preliminary estimates, we must realize distance and velocity matching from $\{\check{v}_1, \check{v}_2, \dots, \check{v}_{K_q}\}$ and $\{\check{r}_1, \check{r}_2, \dots, \check{r}_{K_q}\}$. Specifically, we construct a distance-velocity set as $\Xi_q =$

$\{(\check{r}_1, \check{v}_1), \dots, (\check{r}_1, \check{v}_{K_q}), \dots, (\check{r}_{K_q}, \check{v}_1), \dots, (\check{r}_{K_q}, \check{v}_{K_q})\}$ containing K_q^2 elements. Then the matching value of the element (r_i, v_j) in Ξ_q can be calculated as

$$S_q(r_i, v_j) = |\mathbf{k}_D^H(v_j)\mathbf{H}_q^{RD}\mathbf{k}_R^*(r_i)|. \quad (45)$$

After performing (45) for all r_i and v_j pairs, the set of matching values corresponding to the set Ξ_q can be represented as Ξ_q^S . By searching for the K_q elements with the highest value in Ξ_q^S and their corresponding elements in Ξ_q , we can estimate the distances and velocities of these K_q dynamic targets as $\{(\hat{r}_{q,1}, \hat{v}_{q,1}), (\hat{r}_{q,2}, \hat{v}_{q,2}), \dots, (\hat{r}_{q,K_q}, \hat{v}_{q,K_q})\}$.

Fig. 9 shows examples of distance and velocity estimation and distance-velocity matching under noiseless conditions, for estimation of three targets located in 30° direction set in Fig. 8. The preliminary distance can be estimated from the distance search spectrum in Fig. 9(a) as $90m$, $150m$ and $200m$, while the preliminary velocity can be estimated from the velocity search spectrum as $-25m/s$, $-10m/s$ and $15m/s$. Fig. 9(b) shows the process of distance-velocity matching using (45), and we can obtain the estimation results for the three dynamic targets located in 30° direction, which are $(90m, 30^\circ, 15m/s)$, $(150m, 30^\circ, -10m/s)$ and $(200m, 30^\circ, -25m/s)$.

V. SIMULATION RESULTS

In simulations, we set the number of antennas for transmitting array as $N_T = 128$, the number of antennas for receiving array as $N_R = 128$, the lowest carrier frequency as $f_0 = 220$ GHz and the antenna spacing as $d = \frac{1}{2}\lambda$. The noise is assumed to obey the complex Gaussian distribution with mean $\mu = 0$ and variance $\sigma_n^2 = 1$. The root mean square error (RMSE) of angle estimation, distance estimation, and velocity estimation are defined as $\text{RMSE}_\theta = \sqrt{\frac{\sum_{i=1}^{\text{Count}}(\hat{\theta}_{s(i)} - \theta_s)^2}{\text{Count}}}$, $\text{RMSE}_r = \sqrt{\frac{\sum_{i=1}^{\text{Count}}(\hat{r}_{s(i)} - r_s)^2}{\text{Count}}}$ and $\text{RMSE}_v = \sqrt{\frac{\sum_{i=1}^{\text{Count}}(\hat{v}_{s(i)} - v_s)^2}{\text{Count}}}$, where Count is the number of the Monte Carlo runs, the real parameters of the dynamic target is (r_s, θ_s, v_s) , and $(\hat{r}_{s(i)}, \hat{\theta}_{s(i)}, \hat{v}_{s(i)})$ is the estimation parameters of the target.

The required sensing range of ISAC BS is set as $\{(r, \theta) | r_{\min} \leq r \leq r_{\max}, -60^\circ \leq \theta \leq 60^\circ\}$, in which the range of distance sensing varies slightly in different scenes. We assume that there is clutter everywhere within the sensing range of the BS. The size of the clutter scattering unit is determined by the system's sensing resolution. Specifically, the angle resolution is approximately $\Delta\theta \approx \frac{2}{N_T}$, and the distance resolution is $\Delta r = \frac{c}{2(M-1)\Delta f}$. It is worth pointing out that existing ISAC schemes [15]–[19] that do not consider clutter environment cannot detect the targets and estimate their parameters in actual clutter environment as shown in Fig. 8(a). Thus, we did not show the performance of the existing methods in the simulations.

A. Performance of Dynamic Target Detection

We set that the subcarrier frequency interval is $\Delta f = 200$ kHz, and the number of OFDM symbols is $N = 64$. To test the performance of dynamic target detection, we generate several dynamic targets in each repeated experiment, which are randomly and uniformly distributed within the sensing range

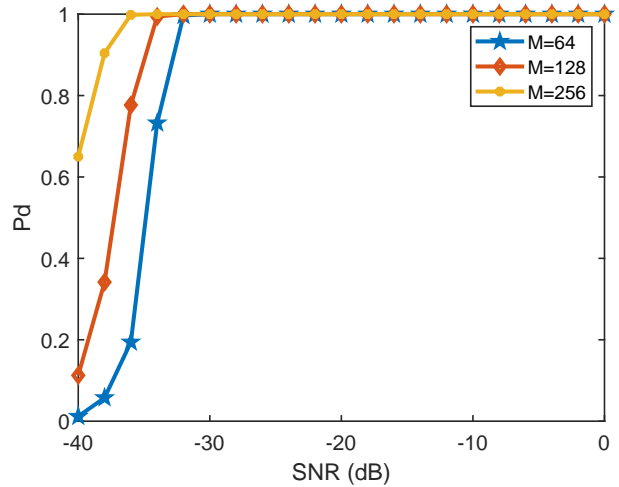


Fig. 10. Curve of dynamic target detection probability versus SNR.

of the BS. Fig. 10 shows the performance curve of dynamic target detection probability P_d over multiple subcarriers with different subcarrier numbers. It can be seen that P_d gradually increases with the increase of SNR. When the SNR is greater than a certain value, P_d can almost approach 100%. In addition, when the SNR is low, P_d increases with the increase of M , which verifies the effectiveness of the proposed joint detection method over multiple subcarriers.

B. Performance of Dynamic Target Parameter Estimation

We assume that the subcarrier frequency interval is $\Delta f = 500$ kHz, the number of OFDM symbols is $N = 64$, and the number of subcarriers is $M = 128$. Fig. 11 shows the curves of sensing RMSE versus SNR for different dynamic targets.

It can be seen from Fig. 11(a) that the RMSE_θ gradually decreases with the increase of SNR. When the SNR is less than -25 dB, the RMSE_θ is large and there is no significant change for RMSE_θ with the change of SNR. As the SNR increases from -25 dB to -10 dB, the RMSE_θ rapidly decreases from 0.15° to 0.01° . As the SNR further increases, the RMSE_θ continues to decrease. In addition, when the distance and velocity parameters are fixed, the closer the angle of the dynamic target approaches 0° , the smaller its RMSE_θ will be. This is mainly because the beam generated by antenna array is narrower near 0° , which improves the performance of angle sensing to some extent.

Fig. 11(b) shows the variation curve of RMSE_r versus SNR, where three dynamic targets are fixed in 20° direction, but their distances are different. It can be seen that when the SNR is low, the RMSE_r remains at a large value, which means that it is difficult to estimate the target parameters under harsh SNR conditions. Nevertheless, when the SNR is greater than 0 dB, the proposed sensing scheme can accurately estimate the distance of the three targets.

Fig. 11(c) shows the RMSE variation curve of target velocity sensing versus SNR. For the target at $50m$, when the SNR reaches -10 dB, its velocity sensing RMSE is about $0.1m/s$. When the SNR increases to 10 dB, the RMSE_v decreases to

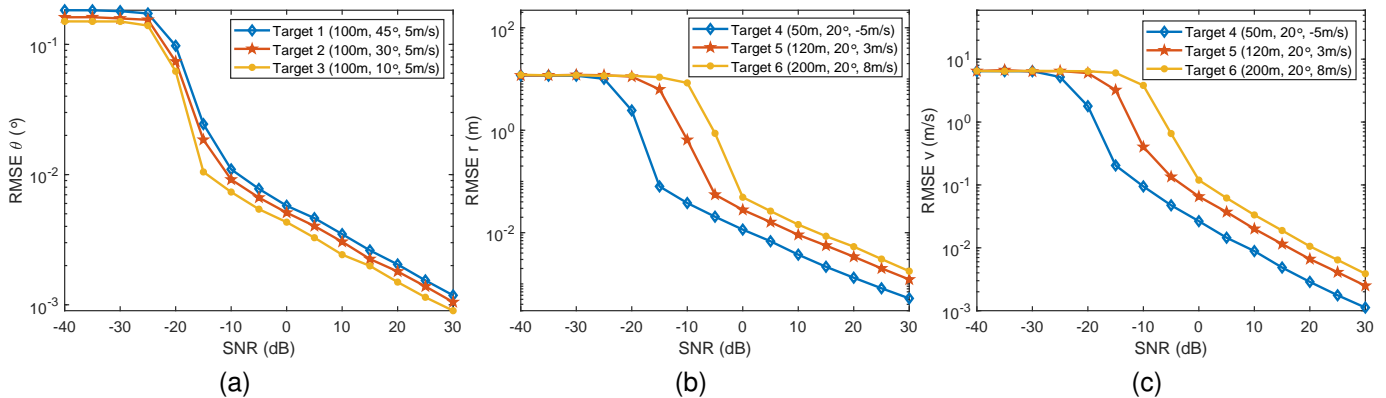


Fig. 11. (a) The RMSE of dynamic target angle sensing; (b) The RMSE of dynamic target distance sensing; (c) The RMSE of dynamic target velocity sensing. The parameter settings for dynamic targets are shown in the figures.

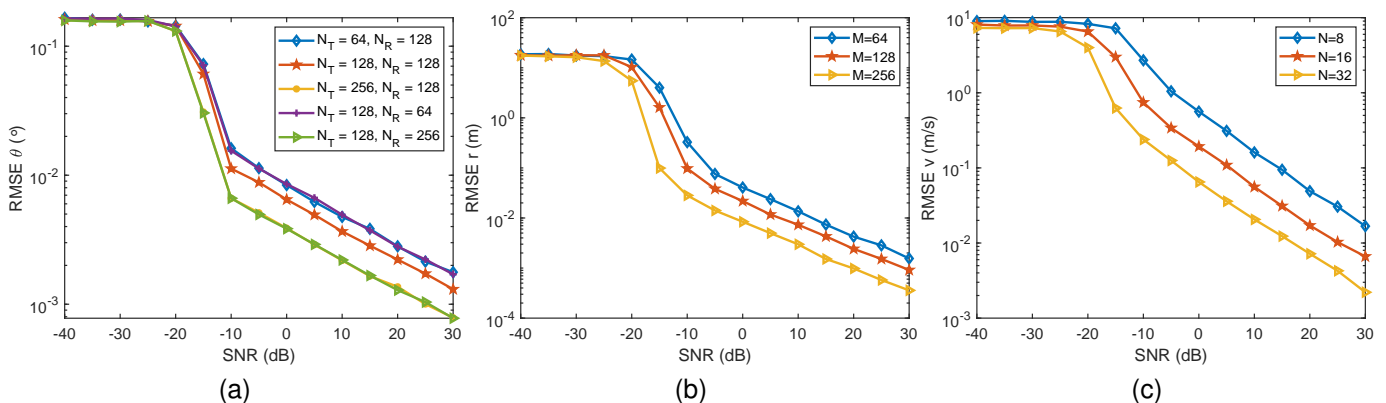


Fig. 12. (a) The RMSE for angle sensing under different array sizes; (b) The RMSE for distance sensing under different numbers of subcarriers; (c) The RMSE for velocity sensing under different numbers of OFDM symbols. The dynamic target is set as $(110m, -20^\circ, 10m/s)$.

$0.01m/s$, which indicates that the proposed sensing scheme has high velocity sensing accuracy.

By comparing the sensing results of three targets at different distances in Fig. 11(b) and Fig. 11(c), we can find that the sensing error of targets at farther distances is larger. This is mainly because the signal power of the dynamic target echo decreases with the increase of target distance, and thus, farther targets will be more susceptible to noise.

C. The Impact of System Resolution on Sensing Performance

The sensing accuracy of a system is usually related to its sensing resolution. Here we will explore the impact of system parameters on sensing resolution and performance.

Fig. 12(a) shows the variation of RMSE versus SNR for angle sensing under different array sizes, in which the subcarrier frequency interval is $\Delta f = 500$ kHz, the number of symbols is $N = 32$ and the number of subcarriers is $M = 128$. It is seen that when the number of transmitting array antennas N_T or the number of receiving array antennas N_R is fixed, the accuracy of angle sensing gradually improves with the increase of N_R or N_T . This phenomenon is mainly because the angle resolution of MIMO systems is inversely proportional to the number of antennas, and more antennas can form narrower beams to provide higher sensing performance.

Fig. 12(b) shows the variation of RMSE versus SNR for distance sensing under different numbers of subcarriers, in which the array size are $N_T = 128$ and $N_R = 128$, subcarrier frequency interval is $\Delta f = 500$ kHz, and the number of OFDM symbols is $N = 32$. It can be seen from the figure that the RMSE of distance sensing significantly decreases with the increase of the number of subcarriers M . In fact, when Δf is fixed, the system transmission bandwidth $W = (M - 1)\Delta f$ linearly increases with M , and the distance resolution $\Delta r = \frac{c}{2B} = \frac{c}{2(M-1)\Delta f}$ gradually decreases in numerical value [41]. Hence, more subcarriers can realize higher distance resolution, which in turn leads to higher distance sensing accuracy.

Fig. 12(c) shows the variation of RMSE versus SNR for velocity sensing under different numbers of OFDM symbols, in which the array size are $N_T = 128$ and $N_R = 128$, subcarrier frequency interval is $\Delta f = 500$ kHz, and the number of subcarriers is $M = 128$. It can be observed that when N is not very large, the accuracy of velocity sensing is already quite satisfactory. In addition, the RMSE of velocity sensing decreases significantly with the increase of N . In reality, when Δf is fixed, the velocity resolution of the system $\Delta v = \frac{c}{2f_0 N T_s}$ decreases as N increases [41]. Hence, more OFDM symbols can bring higher velocity resolution and achieve higher accuracy in velocity sensing.

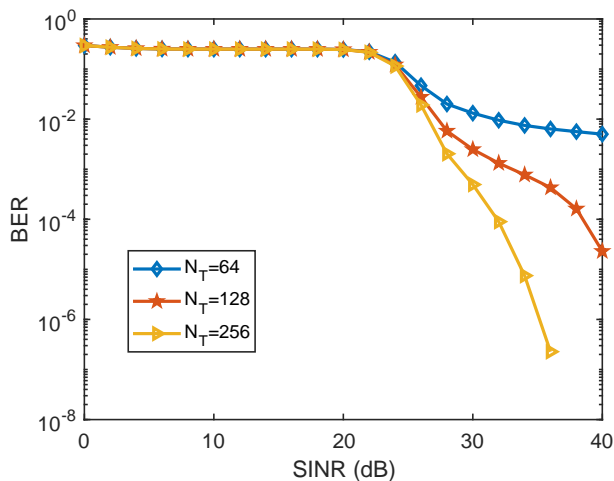


Fig. 13. The curve of BER versus SINR under different array sizes.

D. Communications Performance Evaluation

In this subsection, we will evaluate the communications performance of the proposed ISAC process by using the bit error rate (BER) as the indicator. We set three communication users located in the -40° , 0° , and 30° directions. One sensing beam scans the entire space, and three communications beams communicate with the users for data transmission, in which 16-QAM is employed for communications signals modulation. The number of subcarriers is set to $M = 512$, the subcarrier frequency interval is set to $\Delta f = 480$ kHz, the number of OFDM symbols is set to $N = 64$, and the number of BS transmitting antennas N_T is set as a variable.

Fig. 13 shows the curve of BER versus SINR under different array sizes. It can be seen that when the SINR of the user is high enough, BER gradually decreases as the SINR increases. However, when N_T is small, BER will converge to an error floor as SINR increases. This is mainly because when the antenna array is small, it is difficult to alleviate inter users interference and sensing interference to communications. In addition, it can be found that BER gradually decreases as N_T increases. When N_T is 256 and SINR is 40 dB, the overall BER of communication in the simulation is almost zero.

E. Stability of Sensing Beam Scanning Process

We set the system parameters to $N_T = 128$, $N_R = 128$, $f_0 = 100$ GHz, $P_t = 100$. Besides, we set three users located at $(60m, -40^\circ)$, $(60m, 0^\circ)$ and $(60m, 30^\circ)$, and their minimum SINR requirements are 25 dB, 27 dB, and 30 dB, respectively. Then Fig. 14 shows the performance variation curve of sensing and communications during the sensing beam scanning process. It can be intuitively seen from the figure that the proposed power allocation algorithm can effectively meet the SINR requirements of communications users, while providing satisfactory equivalent sensing power.

VI. CONCLUSIONS

In this paper, we have proposed a practical ISAC framework to sense dynamic targets from clutter environment while

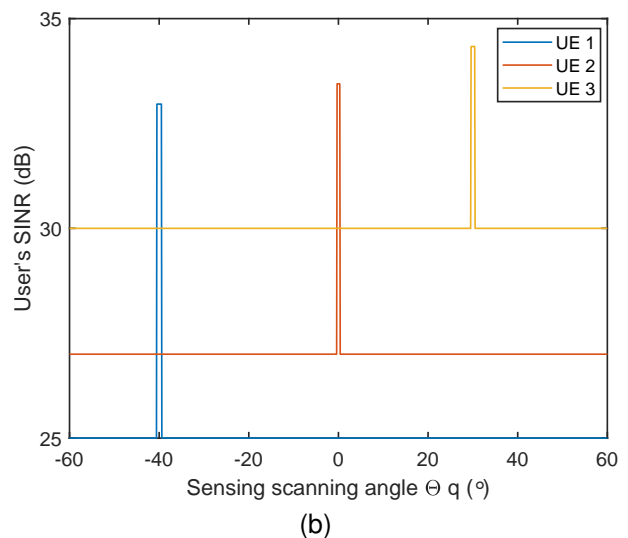
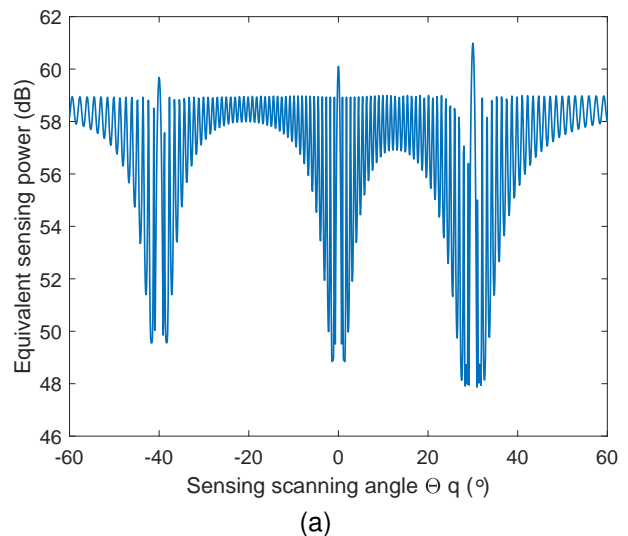


Fig. 14. (a) The variation of equivalent sensing power during SBS process; (b) The variation of user's SINR during SBS process. Three users are set up in the simulation, and their minimum SINR requirements are 25 dB, 27 dB, and 30 dB, respectively.

ensuring users communications quality. In order to implement communications function and sensing function simultaneously, we have designed multiple communications beams that can communicate with the users and one rotating sensing beam can scan the entire space. To minimize the interference of sensing beam on existing communications systems, we have divided the service area into S4S sectors and C4S sectors, and have provided beamforming design and power allocation optimization strategies for each type sector. Then we have proposed the clutter model for ISAC system in urban scenarios and have derived the sensing channel model that includes both static environment and dynamic targets. When BS received echo signals, we first filter out the static environmental clutter and extract the effective dynamic target echoes. Then the task of dynamic target sensing is to detect the presence of dynamic targets and to estimate their angles, distances, and velocities parameters. Among them, dynamic target detection and angle estimation were realized through angle-Doppler spectrum es-

timation and joint detection over multiple subcarriers, while distance and velocity estimation were realized through the extended subspace algorithm. Simulation results have been provided to demonstrate the effectiveness of the proposed schemes and its superiority over the existing methods that ignore clutter environment.

APPENDIX A PROOF OF (36)

To demonstrate the calculation process more clearly, let us ignore the impact of noise, and then $\tilde{h}_{n,m}^{s,q}$ is represented as

$$\begin{aligned}
\tilde{h}_{n,m}^{s,q} &= y_{n,m}^{s,q} / s_{n,m}^{t,q} = \mathbf{w}_{RX,q}^H \mathbf{H}_{n,m} \tilde{\mathbf{x}}_{q,n,m} \\
&= \mathbf{w}_{RX,q}^H \left(\sum_{k=1}^K \mathbf{H}_{k,n,m} + \sum_{i=1}^I \mathbf{H}'_{i,n,m} \right) \tilde{\mathbf{x}}_{q,n,m} \\
&= \sum_{k=1}^K \mathbf{w}_{RX,q}^H \mathbf{H}_{k,n,m} \tilde{\mathbf{x}}_{q,n,m} + \sum_{i=1}^I \mathbf{w}_{RX,q}^H \mathbf{H}'_{i,n,m} \tilde{\mathbf{x}}_{q,n,m} \\
&= \sum_{k=1}^K \alpha_k e^{j\frac{4\pi f_0 v_k T_s}{c} n T_s} e^{-j\frac{4\pi f_m r_k}{c}} \mathbf{w}_{RX,q}^H \mathbf{a}_{RX}(\theta_k) \mathbf{a}_{TX}^H(\theta_k) \tilde{\mathbf{x}}_{q,n,m} \\
&\quad + \sum_{i=1}^I \beta_i e^{-j2\pi f_m \frac{2r'_i}{c}} \mathbf{w}_{RX,q}^H \mathbf{a}_{RX}(\theta'_i) \mathbf{a}_{TX}^H(\theta'_i) \tilde{\mathbf{x}}_{q,n,m}.
\end{aligned} \tag{46}$$

Note that $\mathbf{w}_{RX,q}^H \mathbf{a}_{RX}(\theta_k) \mathbf{a}_{TX}^H(\theta_k) \tilde{\mathbf{x}}_{q,n,m}$ and $\mathbf{w}_{RX,q}^H \mathbf{a}_{RX}(\theta'_i) \mathbf{a}_{TX}^H(\theta'_i) \tilde{\mathbf{x}}_{q,n,m}$ have eliminated the influence of random symbols under massive MIMO array, and thus $\mathbf{w}_{RX,q}^H \mathbf{a}_{RX}(\theta_k) \mathbf{a}_{TX}^H(\theta_k) \tilde{\mathbf{x}}_{q,n,m}$ and $\mathbf{w}_{RX,q}^H \mathbf{a}_{RX}(\theta'_i) \mathbf{a}_{TX}^H(\theta'_i) \tilde{\mathbf{x}}_{q,n,m}$ are independent of n . Then the average of $\tilde{h}_{n,m}^{s,q}$ for the fixed m and q can be calculated as

$$\begin{aligned}
\tilde{h}_{m,q}^{static} &= \tilde{\mathbf{h}}_m^{static}[q] = \frac{1}{N} \sum_{n=0}^{N-1} \tilde{h}_{n,m}^{s,q} \\
&= \frac{1}{N} \sum_{n=0}^{N-1} \left[\sum_{k=1}^K \alpha_k e^{j\frac{4\pi f_0 v_k}{c} n T_s} e^{-j\frac{4\pi f_m r_k}{c}} \mathbf{w}_{RX,q}^H \mathbf{a}_{RX}(\theta_k) \mathbf{a}_{TX}^H(\theta_k) \tilde{\mathbf{x}}_{q,n,m} \right] \\
&\quad + \frac{1}{N} \sum_{n=0}^{N-1} \left[\sum_{i=1}^I \beta_i e^{-j2\pi f_m \frac{2r'_i}{c}} \mathbf{w}_{RX,q}^H \mathbf{a}_{RX}(\theta'_i) \mathbf{a}_{TX}^H(\theta'_i) \tilde{\mathbf{x}}_{q,n,m} \right] \\
&= \frac{1}{N} \sum_{n=0}^{N-1} \left[\sum_{k=1}^K \alpha_k e^{j\frac{4\pi f_0 v_k}{c} n T_s} e^{-j\frac{4\pi f_m r_k}{c}} \mathbf{w}_{RX,q}^H \mathbf{a}_{RX}(\theta_k) \mathbf{a}_{TX}^H(\theta_k) \tilde{\mathbf{x}}_{q,n,m} \right] \\
&\quad + \sum_{i=1}^I \beta_i e^{-j2\pi f_m \frac{2r'_i}{c}} \mathbf{w}_{RX,q}^H \mathbf{a}_{RX}(\theta'_i) \mathbf{a}_{TX}^H(\theta'_i) \tilde{\mathbf{x}}_{q,n,m} \\
&= \sum_{k=1}^K \left[\frac{1}{N} \sum_{n=0}^{N-1} \alpha_k e^{j\frac{4\pi f_0 v_k}{c} n T_s} e^{-j\frac{4\pi f_m r_k}{c}} \mathbf{w}_{RX,q}^H \mathbf{a}_{RX}(\theta_k) \mathbf{a}_{TX}^H(\theta_k) \tilde{\mathbf{x}}_{q,n,m} \right] \\
&\quad + \sum_{i=1}^I \beta_i e^{-j2\pi f_m \frac{2r'_i}{c}} \mathbf{w}_{RX,q}^H \mathbf{a}_{RX}(\theta'_i) \mathbf{a}_{TX}^H(\theta'_i) \tilde{\mathbf{x}}_{q,n,m} \\
&= \sum_{k=1}^K \left[\alpha_k e^{-j\frac{4\pi f_m r_k}{c}} \mathbf{w}_{RX,q}^H \mathbf{a}_{RX}(\theta_k) \mathbf{a}_{TX}^H(\theta_k) \tilde{\mathbf{x}}_{q,n,m} \frac{1}{N} \sum_{n=0}^{N-1} e^{j\frac{4\pi f_0 v_k}{c} n T_s} \right] \\
&\quad + \sum_{i=1}^I \beta_i e^{-j2\pi f_m \frac{2r'_i}{c}} \mathbf{w}_{RX,q}^H \mathbf{a}_{RX}(\theta'_i) \mathbf{a}_{TX}^H(\theta'_i) \tilde{\mathbf{x}}_{q,n,m}.
\end{aligned} \tag{47}$$

Since

$$\begin{aligned}
&\lim_{N \rightarrow \infty} \frac{1}{N} \sum_{n=0}^{N-1} e^{j\frac{4\pi f_0 v_k}{c} n T_s} \\
&= \lim_{N \rightarrow \infty} \left[\frac{1}{N} e^{j\frac{2\pi f_0 v_k T_s (N-1)}{c}} \frac{\sin(2\pi f_0 v_k T_s N/c)}{\sin(2\pi f_0 v_k T_s/c)} \right] = 0,
\end{aligned} \tag{48}$$

there is

$$\begin{aligned}
\lim_{N \rightarrow \infty} \tilde{h}_{m,q}^{static} &= \lim_{N \rightarrow \infty} \frac{1}{N} \sum_{n=0}^{N-1} \tilde{h}_{n,m}^{s,q} \\
&= \sum_{i=1}^I \beta_i e^{-j2\pi f_m \frac{2r'_i}{c}} \mathbf{w}_{RX,q}^H \mathbf{a}_{RX}(\theta'_i) \mathbf{a}_{TX}^H(\theta'_i) \tilde{\mathbf{x}}_{q,n,m} \\
&= \mathbf{w}_{RX,q}^H \left(\sum_{i=1}^I \mathbf{H}'_{i,n,m} \right) \tilde{\mathbf{x}}_{q,n,m}.
\end{aligned} \tag{49}$$

Then Eq. (36) has been proven.

REFERENCES

- [1] F. Liu, Y. Cui, C. Masouros, J. Xu, T. X. Han, Y. C. Eldar, and S. Buzzi, "Integrated sensing and communications: Toward dual-functional wireless networks for 6G and beyond," *IEEE J. Sel. Areas Commun.*, vol. 40, no. 6, pp. 1728–1767, Jun. 2022.
- [2] M. Giordani, M. Polese, M. Mezzavilla, S. Rangan, and M. Zorzi, "Toward 6G networks: Use cases and technologies," *IEEE Commun. Mag.*, vol. 58, no. 3, pp. 55–61, Mar. 2020.
- [3] C. De Lima *et al.*, "Convergent communication, sensing and localization in 6G systems: An overview of technologies, opportunities and challenges," *IEEE Access*, vol. 9, pp. 26902–26925, Jan. 2021.
- [4] C. Chaccour, M. N. Soorki, W. Saad, M. Bennis, P. Popovski, and M. Debbah, "Seven defining features of terahertz (THz) wireless systems: A fellowship of communication and sensing," *IEEE Commun. Surveys Tuts.*, vol. 24, no. 2, pp. 967–993, Jan. 2022.
- [5] Z. Wei, F. Liu, C. Masouros, N. Su, and A. P. Petropulu, "Toward multi-functional 6G wireless networks: Integrating sensing, communication, and security," *IEEE Commun. Mag.*, vol. 60, no. 4, pp. 65–71, Apr. 2022.
- [6] J. Yang, C.-K. Wen, and S. Jin, "Hybrid active and passive sensing for SLAM in wireless communication systems," *IEEE J. Sel. Areas Commun.*, vol. 40, no. 7, pp. 2146–2163, Jul. 2022.
- [7] J. Yang and *et al.*, "Enabling plug-and-play and crowdsourcing SLAM in wireless communication systems," *IEEE Trans. Wireless Commun.*, vol. 21, no. 3, pp. 1453–1468, Mar. 2022.
- [8] H. Que, J. Yang, C.-K. Wen, S. Xia, X. Li, and S. Jin, "Joint beam management and SLAM for mmWave communication systems," *IEEE Trans. Commun.*, pp. 1–1, Jul. 2023.
- [9] H. Chen, H. Sarrieddeen, T. Ballal, H. Wymeersch, M.-S. Alouini, and T. Y. Al-Naffouri, "A tutorial on terahertz-band localization for 6G communication systems," *IEEE Commun. Surveys Tuts.*, vol. 24, no. 3, pp. 1780–1815, May 2022.
- [10] Z. Lin, T. Lv, J. A. Zhang, and R. P. Liu, "3D wideband mmwave localization for 5G massive MIMO systems," in *Proc. IEEE Global Commun. Conf. (GLOBECOM)*, Waikoloa, HI, USA, Dec. 2019, pp. 1–6.
- [11] O. Kanhere and T. S. Rappaport, "Position location for futuristic cellular communications: 5G and beyond," *IEEE Commun. Mag.*, vol. 59, no. 1, pp. 70–75, Jan. 2021.
- [12] X. Ma, T. Ballal, H. Chen, O. Aldayel, and T. Y. Al-Naffouri, "A maximum-likelihood TDOA localization algorithm using difference-of-convex programming," *IEEE Signal Process. Lett.*, vol. 28, pp. 309–313, Jan. 2021.
- [13] H. Chen, T. Ballal, N. Saeed, M.-S. Alouini, and T. Y. Al-Naffouri, "A joint TDOA-PDOA localization approach using particle swarm optimization," *IEEE Wireless Commun. Lett.*, vol. 9, no. 8, pp. 1240–1244, Aug. 2020.
- [14] H. Chen, T. Ballal, and T. Y. Al-Naffouri, "DOA estimation with non-uniform linear arrays: A phase-difference projection approach," *IEEE Wireless Commun. Lett.*, vol. 10, no. 11, pp. 2435–2439, Nov. 2021.

- [15] Z. Gao, Z. Wan, D. Zheng, S. Tan, C. Masouros, D. W. K. Ng, and S. Chen, "Integrated sensing and communication with mmWave massive MIMO: A compressed sampling perspective," *IEEE Trans. Wireless Commun.*, vol. 22, no. 3, pp. 1745–1762, Mar. 2023.
- [16] Z. Wang, X. Mu, and Y. Liu, "STARS enabled integrated sensing and communications," *IEEE Trans. Wireless Commun.*, pp. 1–1, Feb. 2023.
- [17] Y. Li, X. Wang, and Z. Ding, "Multi-target position and velocity estimation using OFDM communication signals," *IEEE Trans. Commun.*, vol. 68, no. 2, pp. 1160–1174, Feb. 2020.
- [18] P. Kumari, J. Choi, N. González-Prelcic, and R. W. Heath, "IEEE 802.11ad-based radar: An approach to joint vehicular communication-radar system," *IEEE Trans. Veh. Technol.*, vol. 67, no. 4, pp. 3012–3027, Apr. 2018.
- [19] X. Chen, Z. Feng, Z. Wei, X. Yuan, P. Zhang, J. Andrew Zhang, and H. Yang, "Multiple signal classification based joint communication and sensing system," *IEEE Trans. Wireless Commun.*, pp. 1–1, 2023.
- [20] X. Liu, T. Huang, N. Shlezinger, Y. Liu, J. Zhou, and Y. C. Eldar, "Joint transmit beamforming for multiuser MIMO communications and MIMO radar," *IEEE Trans. Signal Process.*, vol. 68, pp. 3929–3944, Jun. 2020.
- [21] D. Luo, Z. Ye, and J. Zhu, "Secure transmit beamforming for radar-communication systems using NOMA," *IEEE Commun. Lett.*, vol. 26, no. 11, pp. 2557–2561, Nov. 2022.
- [22] D. Cong, S. Guo, H. Zhang, J. Ye, and M.-S. Alouini, "Beamforming design for integrated sensing and communication systems with finite alphabet input," *IEEE Wireless Commun. Lett.*, vol. 11, no. 10, pp. 2190–2194, Oct. 2022.
- [23] Z. He, W. Xu, H. Shen, Y. Huang, and H. Xiao, "Energy efficient beamforming optimization for integrated sensing and communication," *IEEE Wireless Commun. Lett.*, vol. 11, no. 7, pp. 1374–1378, Jul. 2022.
- [24] C. B. Barneto, T. Riihonen, S. D. Liyanaarachchi, M. Heino, N. González-Prelcic, and M. Valkama, "Beamformer design and optimization for joint communication and full-duplex sensing at mm-Waves," *IEEE Trans. Commun.*, vol. 70, no. 12, pp. 8298–8312, Dec. 2022.
- [25] H. Luo, R. Liu, M. Li, Y. Liu, and Q. Liu, "Joint beamforming design for RIS-assisted integrated sensing and communication systems," *IEEE Trans. Veh. Technol.*, vol. 71, no. 12, pp. 13393–13397, Dec. 2022.
- [26] X. Wang, Z. Fei, J. A. Zhang, and J. Xu, "Partially-connected hybrid beamforming design for integrated sensing and communication systems," *IEEE Trans. Commun.*, vol. 70, no. 10, pp. 6648–6660, Oct. 2022.
- [27] H. Luo, F. Gao, W. Yuan, and S. Zhang, "Beam squint assisted user localization in near-field integrated sensing and communications systems," *IEEE Trans. Wireless Commun.*, pp. 1–1, Oct. 2023.
- [28] D. Shnidman, "Generalized radar clutter model," *IEEE Trans. Aerosp. Electron. Syst.*, vol. 35, no. 3, pp. 857–865, Jul. 1999.
- [29] J. Billingsley *et al.*, "Statistical analyses of measured radar ground clutter data," *IEEE Trans. Aerosp. Electron. Syst.*, vol. 35, no. 2, pp. 579–593, Apr. 1999.
- [30] D. Barton, "Land clutter models for radar design and analysis," *Proceedings of the IEEE*, vol. 73, no. 2, pp. 198–204, Feb. 1985.
- [31] M. I. Skolnik, "Radar handbook," 3rd ed. New York, NY, USA: McGraw-Hill, 2008.
- [32] F. Liu, L. Zhou, C. Masouros, A. Li, W. Luo, and A. Petropulu, "Toward dual-functional radar-communication systems: Optimal waveform design," *IEEE Trans. Signal Process.*, vol. 66, no. 16, pp. 4264–4279, Aug. 2018.
- [33] C. B. Barneto, T. Riihonen, S. D. Liyanaarachchi, M. Heino, N. González-Prelcic, and M. Valkama, "Beamformer design and optimization for joint communication and full-duplex sensing at mm-waves," *IEEE Trans. Commun.*, vol. 70, no. 12, pp. 8298–8312, Dec. 2022.
- [34] M. Grant and S. Boyd, "CVX: Matlab software for disciplined convex programming, version 2.1." <http://cvxr.com/cvx>, Mar. 2014.
- [35] D. Luo, Z. Ye, B. Si, and J. Zhu, "Secure transmit beamforming for radar-communication system without eavesdropper CSI," *IEEE Trans. Veh. Technol.*, vol. 71, no. 9, pp. 9794–9804, Sep. 2022.
- [36] C. Sturm and W. Wiesbeck, "Waveform design and signal processing aspects for fusion of wireless communications and radar sensing," *Proceedings of the IEEE*, vol. 99, no. 7, pp. 1236–1259, Jul. 2011.
- [37] T. Multerer, M. Vossiek, U. Prechtel, and V. Ziegler, "Spectrum-efficient real-time OFDM MIMO radar for moving target detection in medium-range applications," in *Proc. IEEE MTT-S Int. Microw. Symp. Dig.*, Munich, Germany, Aug. 2018, pp.1–4.
- [38] H. Rohling, "Radar CFAR thresholding in clutter and multiple target situations," *IEEE Trans. Aerosp. Electron. Syst.*, vol. AES-19, no. 4, pp. 608–621, Jul. 1983.
- [39] M. Wax and T. Kailath, "Detection of signals by information theoretic criteria," *IEEE Trans. Acoust., Speech, Signal Process.*, vol. 33, no. 2, pp. 387–392, Apr. 1985.
- [40] A. Barron, J. Rissanen, and B. Yu, "The minimum description length principle in coding and modeling," *IEEE Trans. Inf. Theory*, vol. 44, no. 6, pp. 2743–2760, Oct. 1998.
- [41] K. B. S. A. Dapa, G. Point, S. Bensator, and F. E. Boukour, "Vehicular communications over OFDM radar sensing in the 77 GHz mmWave band," *IEEE Access*, vol. 11, pp. 4821–4829, Jan. 2023.